iScience

CellPress
OPEN ACCESS

Article

Intergenerational epigenetic inheritance mediated by MYS-2/MOF in the pathogenesis of Alzheimer's disease

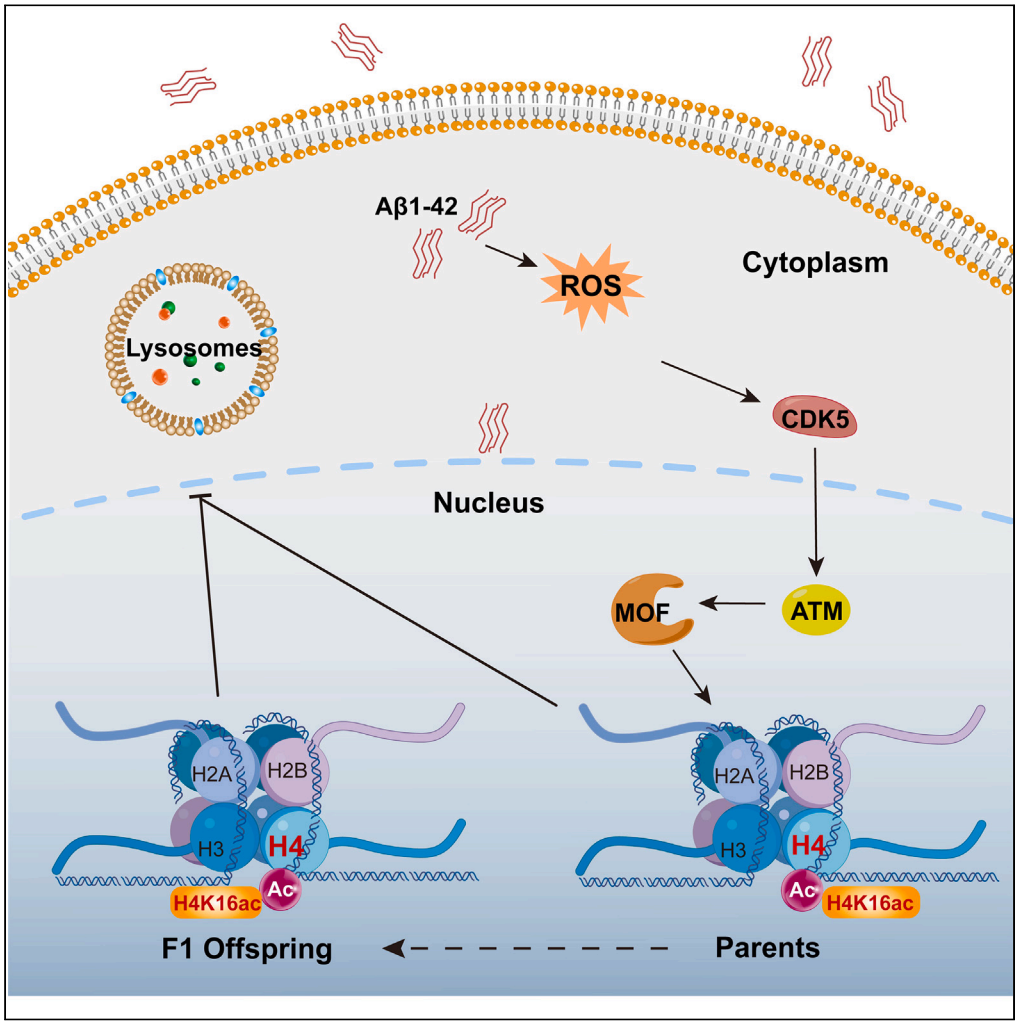

Yuhong Li, Hua Bai, Wenwen Liu, ..., Xinyi Yan, Ninghui Zhao, Xiaowei Huang

zhaoninghui@hotmail.com (N.Z.)
xwhuang@ynu.edu.cn (X.H.)

Highlights

H4K16ac could be inherited intergenerationally via MYS-2/MOF in AD model

P0 and F1 generation had the similar H4K16ac and gene expression in AD-related pathways

The ROS/CDK-5/ATM pathway functioned as an upstream activator of MYS-2/MOF

Li et al., iScience 27, 110588
August 16, 2024
https://doi.org/10.1016/j.isci.2024.110588

iScience

CellPress
OPEN ACCESS

Article

Intergenerational epigenetic inheritance mediated by MYS-2/MOF in the pathogenesis of Alzheimer's disease

Yuhong Li,[1,2,5] Hua Bai,[1,3,5] Wenwen Liu,[1,5] Wenhui Zhou,[1] Huan Gu,[1] Peiji Zhao,[1] Man Zhu,[1,2] Yixin Li,[1] Xinyi Yan,[1] Ninghui Zhao,[4,*] and Xiaowei Huang[1,6,*]

SUMMARY

Although autosomal-dominant inheritance is believed an important cause of familial clustering Alzheimer's disease (FAD), it covers only a small proportion of FAD incidence, and so we investigated epigenetic memory as an alternative mechanism to contribute for intergenerational AD pathogenesis. Our data *in vivo* showed that mys-2 of *Caenorhabditis elegans* that encodes a putative MYST acetyltransferase responsible for H4K16 acetylation modulated AD occurrence. The phenotypic improvements in the parent generation caused by mys-2 disfunction were passed to their progeny due to epigenetic memory, which resulted in similar H4K16ac levels among the candidate target genes of MYS-2 and similar gene expression patterns of the AD-related pathways. Furthermore, the ROS/CDK-5/ATM pathway functioned as an upstream activator of MYS-2. Our study indicated that MYS-2/MOF could be inherited intergenerationally via epigenetic mechanisms in *C. elegans* and mammalian cell of AD model, providing a new insight into our understanding of the etiology and inheritance of FAD.

INTRODUCTION

Alzheimer's disease (AD) is an irreversible neurodegenerative disease characterized by progressive cognitive decline due to degeneration of synapses and axons.[1] Aging is the strongest risk factor for development of AD and effective treatment options are lacking. Therefore, AD research has received a great deal of attention due to the aging nature of society. Approximately 50 million individuals had AD worldwide in 2018, with the number expected to reach 150 million in 2050.[2]

A number of genetic factors have been associated with AD pathogenesis, particularly in cases of familial clustering AD (FAD). Familiar clustering AD, defined as two or more successive generations of a family member with AD, accounts for about 12.5–25% of all AD cases.[3] Pedigree studies have suggested that autosomal-dominant forms of FAD originate mostly from mutations among one of three genes: amyloid precursor protein (APP), presenilin 1 (PSEN1), and presenilin 2 (PSEN2).[4,5] Missense mutations in these genes disrupts processing of APP, resulting in excessive production and accumulation of amyloid-β (Aβ) and neuronal degeneration in the central nervous system. However, the incidence rate of autosomal-dominant inheritance is less than 50% in FAD according to an epidemiological survey of Caucasians.[6,7] In Asian populations, PSENs/APP mutations occur even less frequently than those in Caucasians, with 11.11% detected in Japanese[8] and 16.70% in Korean.[9] A recent report from 404 Chinese FAD showed that 83.17% of pedigrees carry no PSENs/APP mutations, which indicated involvement of other candidate genes or alternative mechanisms of non-autosomal dominant inheritance.[10]

Epigenetic mechanisms play major roles AD development by changing the expression patterns of pathogenic genes.[11,12] Moreover, they also link external risk factors to internal changes. Environmental/behavioral factors, such as pesticide exposure, high-fat diet, and sedentary lifestyle have been associated with epigenomic remodeling increased incidence of AD.[13–15] Among epigenetic mechanisms, histone acetylases (HATs) and histone deacetylases (HDACs) reversibly transfer acetyl groups to lysine residues of histone N-termini, resulting in chromatin being open or compact with regard to transcriptional factors access. Amyloid β has been shown to stimulate HAT activity, and sequentially enhanced H3 acetylation.[16,17] On the other hand, AD-related genes, such as Psen1, Bace1, Ncstn, and Adora2a, were also upregulated in hippocampal and cortical neurons due to the enhanced H3 acetylation in their promoter regions.[18,19] In contrast, loss of a HAT Tip60 increased the transcriptional expression of APP and induced neuronal apoptosis in APP transgenic Drosophila.[20] Histone deacetylases (HDACs) have been associated with several hallmarks of AD, including tau accumulation, neuronal loss, and impairment of the parietal cortex

[1]School of Medicine, State Key Lab for Conservation and Utilization of Bio-Resources, Yunnan University, Kunming 650091, China
[2]College of Biological Resources and Food Engineering, Qujing Normal University, Qujing 655000, China
[3]School of Public Health, Kunming Medical University, Kunming 650500, China
[4]Neurosurgery of the Second Hospital Affiliated with Kunming Medical University, Kunming 650101, China
[5]These authors contributed equally
[6]Lead contact
*Correspondence: zhaoninghui@hotmail.com (N.Z.), xwhuang@ynu.edu.cn (X.H.)
https://doi.org/10.1016/j.isci.2024.110588

due to reduced sirtuin 1 (SIRTl, a member of the HDAC class III family) activity.[21,22] Though acetylation of H4 histone regulates a variety of biological processes that are closely correlate with AD, such as learning,[23] memory,[24] and aging,[25,26] the role of H4 acetylation and its underlying molecular pathways need to be further elucidated in AD pathogenesis.

Caenorhabditis elegans has been used as a powerful tool to investigate the intergenerational epigenetic effects of complex biological activities, such as longevity,[27] mitochondrial stress adaptations transmission,[28] and learning pathogenic avoidance.[29,30] Furthermore, some epigenetic mechanisms operating within the germline cycle of *C. elegans* also influence gene expression in somatic lineages.[31] At the same time, since *C. elegans* that typically expresses the transgenic disease-associated human proteins can recapitulate the phenotypic aspects of human diseases. The transgenic AD model of *C. elegans* has already proven its great values in drug screening and for better understanding of the cellular mechanisms such as Aβ formation and clearance.[32–34] Moreover, H4K16ac was recently shown to be intergenerationally transmitted from the female germline, which raises an intriguing possibility that maternal H4K16ac may be a "blueprint" for embryonic development.[35] So here, we used both *C. elegans* and mammalian cell AD model to investigate a possible involvement of epigenetic inheritance in AD pathogenesis.

RESULTS

Involvement of a putative MYST acetyltransferase MYS-2 in AD pathogenesis in *C. elegans*

To investigate whether H4 histone acetylation contributed to AD pathogenesis, we evaluated key genes involved in acetylation or deacetylation of H4 histone N-termini (i.e., *hat-1*, *mys-2*, *anat-1*, and *sir-2.1*) in a *C. elegans* AD model CL4176 by feeding the specific RNA interference (RNAi) bacteria.[36,37] Compared to the non-paralysis phenotype in the negative-control CL802 that lacked Aβ peptide expression, the transgenic CL4176 nematodes became paralyzed within 22 h after a temperature shift from 16°C to 25°C.[38] However, only *mys-2* RNAi significantly reduced paralysis and delayed AD pathogenesis (Figure 1A). In addition, mutation of *mys-2* decreased the paralytic rates in a double-transgenic germline CL4176;*mys-2(ok2429)* more significantly. (Figure 1B). Next, we expressed P*mys-2*:GFP in CL4176 which expressed Aβ in body wall muscle and observed the ubiquitous expression of *mys-2*, including the body wall musculature same to the localization of Aβ (Figure S1).

To further confirm the involvement of gene *mys-2* in AD pathogenesis, CL4176 nematodes were treated with MG149, an inhibitor of the mammalian ortholog MOF,[39] in L3 stage until laying eggs. Treatment with MG149 (50 μM) reduced the proportion of paralyzed nematodes (Figure 1C). As *sumv-1* has been shown to form a KAT8/MOF-like complex with MYS-2 in *C. elegans*,[40] paralytic rates were compared between CL4176 nematodes treated with *sumv-1* and *mys*-2 RNAi. The results showed that both RNAi similarly reduced pathogenesis of AD (Figure 1D), suggesting MYS-2 and its complex should be involved in the AD model of CL4176.

Since MOF, the mammalian ortholog of MYS-2, functions as an acetyltransferase for H4K16ac in mammals,[41,42] we hypothesized that MYS-2 was a putative acetyltransferase in *C. elegans* and determined the acetylation levels of H4K16 in both negative control CL802 and AD model CL4176. Western-blot analysis showed that CL4176 had significantly higher H4K16ac levels than CL802 control nematodes (Figure 1E) but had little effect on H3K9ac (Figure S2A). As expected, mutation of *mys-2* significantly repressed H4K16ac in the CL4176 nematodes (Figure 1F) and did not change H3K9ac (Figure S2B), which raises the possibility that acetylation of H4K16 mediated by *mys-2* may be involved in AD pathogenesis in *C. elegans*.

Intergenerational heredity of AD pathogenesis mediated by *mys-2*

Recently, MYS-2 was shown to maintain transgenerational H4K16ac and to act as a "blueprint" for embryonic development.[35] Therefore, we evaluated whether *mys-2* also controlled intergenerational inheritance of AD pathogenesis. The results showed that the progeny of the *mys-2* knockdown parental generation (P0) showed reduced paralysis rates compared to those of wild-type CL4176 nematodes until at least F2 (Figure 2A). However, this intergenerational reduction in paralysis rate was not due to RNAi in the progeny because qPCR data showed significantly reduced *mys-2* level in the P0 generation in response *mys-2* RNAi, but no change was detected in F1 descendants (Figure 2B). Moreover, to avoid the possible effects of exogenous RNA on F1 descendants of P0 generation treated with *mys-2* RNAi,[43] we replaced *mys-2* RNAi treatment with administration of the inhibitor MG149 to the P0 generation only. Reanalysis of paralysis rates showed that the P0 generation to F2 progeny showed the similar delayed paralysis (Figure 2C). We also detected that MG149 was not residue in the offspring (Figure S3; Table S1). Consistent with the paralysis phenotypes, P0 and F1 generations treated with either *mys-2* RNAi or the inhibitor MG149 had decreased levels of H4K16ac (Figures 2D and 2E), indicating *mys-2* mediated the decrease of H4K16ac level and thus played a role in the intergenerational inheritance of AD.

As Aβ expression might be affected by the chromatin modification caused by *mys-2* disturbance or other factors, we evaluated Aβ1-42 expressional levels in CL4176 nematodes under the following conditions: CL4176;*mys-2(ok2429)*, *mys-2* RNAi P0 generation, F1-F3 generations, *sumv-1* RNAi, and MG149 treatment. Quantitative PCR results showed no significant differences in the expression of Aβ under the all conditions (Figure S4A), indicating that the reduced paralysis rates were not due to the reduced Aβ1-42 transcripts.

F1 progeny with epigenetic memory had similar gene expression patterns to P0 generation

Because of the similar AD phenotype and heritability of H4K16ac among the P0 generation and its progeny F1, we evaluated whether these similarities were due to epigenetic inheritance. RNA-seq was performed on the following CL4176 strains: P0 generation with *mys-2* mutation (CL4176;*mys-2(ok2429)*) and F1 descendants of the *mys-2*-RNAi-treated P0 generation. The differentially expressed genes were statistically analyzed in the P0 generation (CL4176;*mys-2(ok2429)* vs. CL4176) and F1 generations (CL4176;*mys-2* RNAi in P0 vs. CL4176), respectively.

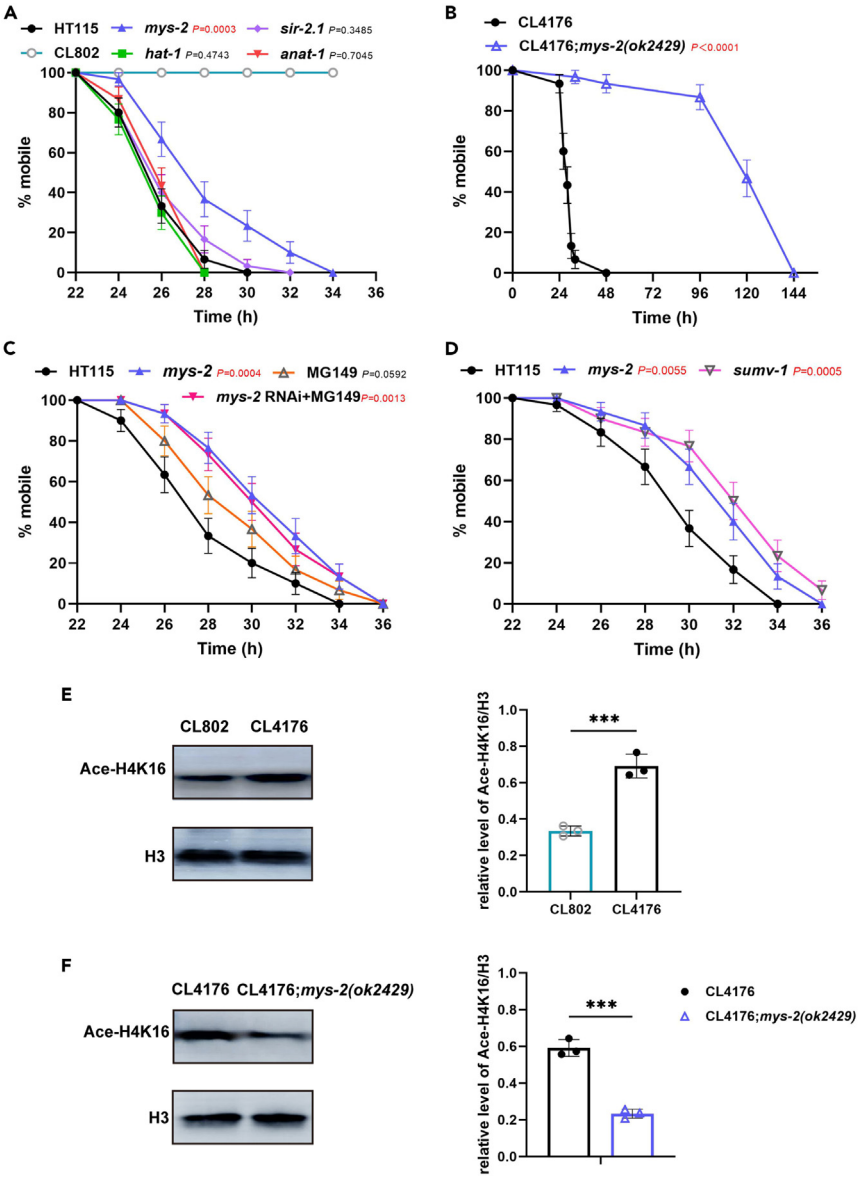

Figure 1. H4K16ac mediated by the *mys-2* gene contributed to AD pathogenesis

(A) Among a series of genes that had potential effects on H4 histone acetylation, *mys-2* RNAi reduced the paralysis rate in CL4176 *C. elegans*.

(B) Mutation of *mys-2* gene significantly delayed onset of paralysis and reduced paralysis rates.

(C) Addition of the MOF inhibitor, MG149 (50 μM), reduced the proportion of paralyzed nematodes.

(D) Interference of the *sumv-1* gene, which forms a KAT8/MOF-like complex with MYS-2, ameliorated the paralytic phenotype. *p* value presented as the comparison with HT115 or CL4176.

(E) Western-blot analysis using a histone H4K16-acetylation antibody showed that increased levels of H4K16ac in CL4176 nematodes compared to those in the CL802 negative control.

(F) Mutation of the *mys-2* gene in CL4176 significantly reduced H4K16ac.

Furthermore, the linear correlation coefficient of the differentially expressed genes between P0 generation and F1 progeny was 0.8313 (Figure 3A), indicating that F1 progeny maintained comparable gene expression patters to the P0 generation through epigenetic modification. Similarly, there was no significant differences in the levels of Aβ1-42 among CL4176 and *mys-2* loss function groups of sequenced samples that was consistent with the qPCR result of Aβ (Figure S4B; Table S2), suggesting the disfunction of *mys-2* improve paralysis without influence on the expression level of Aβ1-42 between generations.

To identify candidate genes for improving AD pathogenesis in the P0 and F1 generations, we categorized DEGs using either Panther GO-SLIM or Kyoto encyclopedia of genes and genomes (KEGG). The results showed that the DEGs in the P0 and F1 generations shared the same

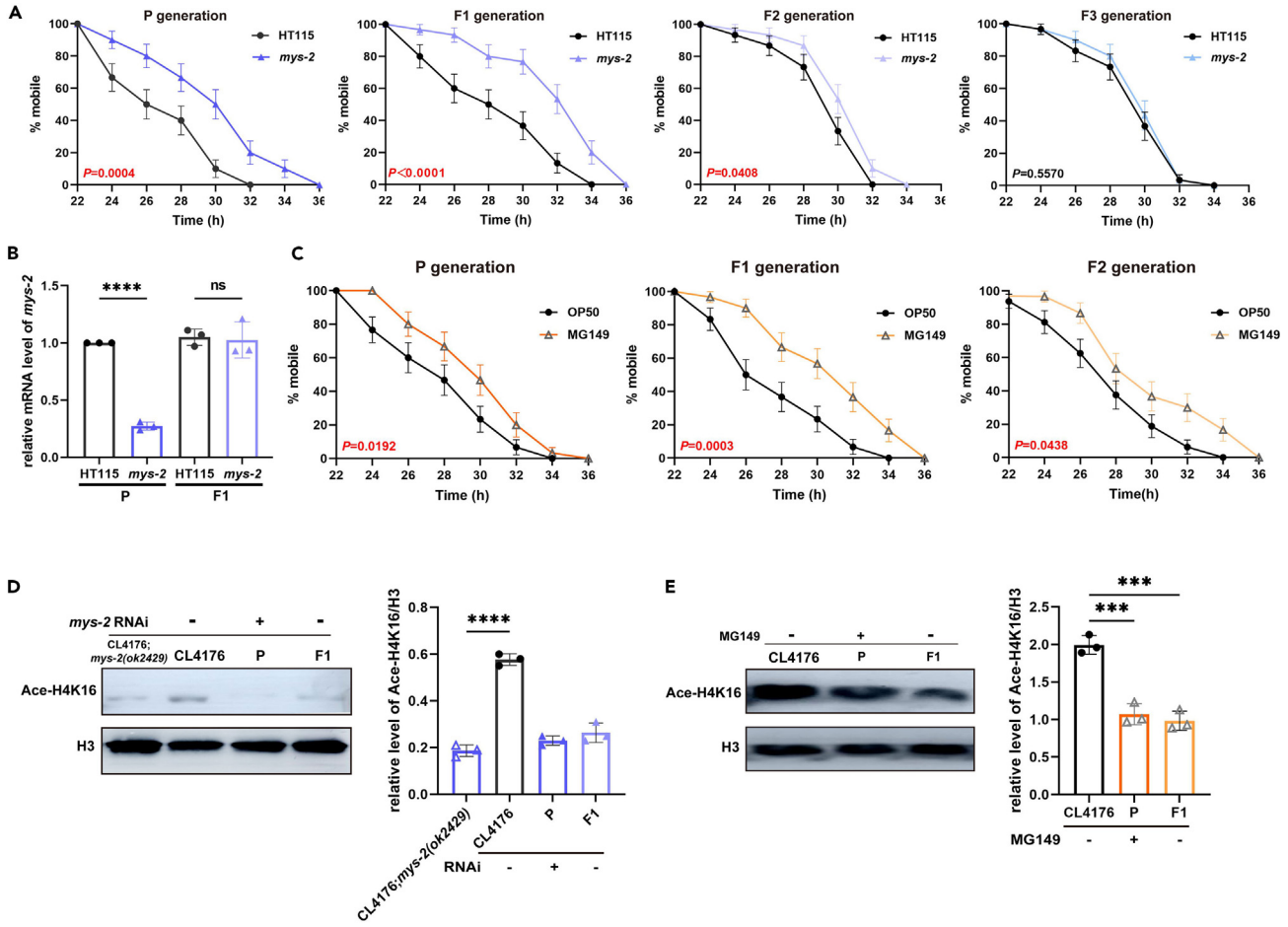

Figure 2. H4K16ac mediated by the *mys-2* gene contributed to intergenerational inheritance of AD

(A) Reduced paralysis of CL4176 nematodes caused by *mys-2* RNAi in the P0 generation was inherited by progeny.

(B) The mRNA levels of *mys-2* were assessed in the HT115 negative control, in the P0 generation treated with *mys-2* RNAi, and in the F1 generation.

(C) F1 and F2 progeny from the P0 generation treated with MG149 also showed delayed paralysis.

(D and E) Reduced H4K16ac levels were observed in CL4176;*mys-2(ok2429)* nematodes and in the P0 generation treated with *mys-2* RNAi (D) or MG149 (E), and F1 progeny.

pathways associated with neurodegenerative diseases, including AD, Parkinson's disease (PD), and Huntington's disease (HD) (Figure 3B; Figure S5A). Several biological processes closely related to AD pathogenesis, such as apoptosis,[44] ubiquitin proteasomes,[45] angiogenesis,[46] Wnt signaling,[47] TGF-β signaling,[48] PI3 kinase signaling,[49] platelet-derived growth factor (PDGF),[50] and cadherin signaling[51] share the similar pathways in P0 and F1 (Figure S5A). In addition, the shared top 100 upregulated genes and the total shared upregulated genes between the P0 and F1 generations were enriched in biological functions such as sugar metabolism, lipid metabolism, autophagy, and lysosome that had the potential roles in AD pathogenesis (Figure 3C; Figure S5B).

F1 progeny imitated the similar H4K16 acetylation and gene expression of P0 generation in AD-related pathways

To confirm that F1 progeny recapitulated the gene-expression patterns of the P0 generation, a few candidate genes were chosen from the enriched pathways in our transcriptome data (Figures S6A and S6B). We used qPCR to quantify downregulated genes in AD-like pathophysiology (e.g., *ttr-41*, *acs-4*, *y48c3a.5*, *h14e04.2*, and *glh-2*) (Figure 4A) and upregulated genes related to lysozymes (e.g., *lys-4*, *lys-5*, *lys-6*, *lys-10*, *ilys-2*, and *ilys-3*) (Figure 4B), fatty metabolism (e.g., *lips-6*, *oac-15*, *oac-35*, *oac-36*, and *oac-56*) (Figure S6C), and sugar metabolism (e.g., *glct-4*, *c47f8.6*, *clec-60*, *c47f8.5*, *gmd-2*, *e03h4.11*, and *bgnt-1.8*) (Figure S6D). The results showed the significant similarities in the expression levels of enriched pathway genes between P0 and F1.

To establish the correlation between gene expression and promoter region acetylation of H4, chromatin immunoprecipitation-quantitative real-time PCR (ChIP-qPCR) was performed on candidate genes from CL4176, CL4176;*mys-2* RNAi in P0 and its F1 progeny. The search strategy for enriched motifs from the differentially expressed genes was as follows. Promoter regions were extracted from 2,000-base pair (bp)

A

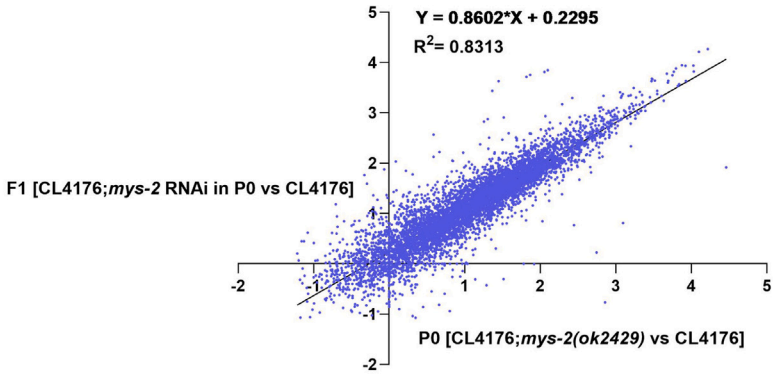
log10(FPKM): log 10 of PFKM value of significantly different expression genes
Y = 0.8602*X + 0.2295
R2= 0.8313
F1 [CL4176;mys-2 RNAi in P0 vs CL4176]
P0 [CL4176;mys-2(ok2429) vs CL4176]

B

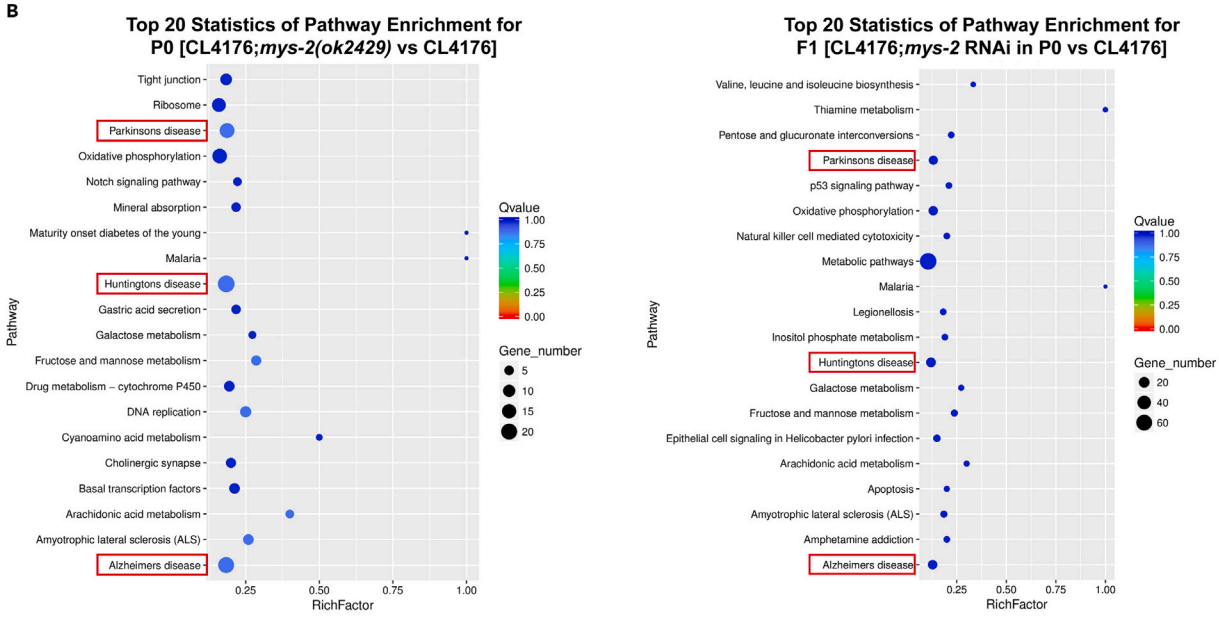
Top 20 Statistics of Pathway Enrichment for
P0 [CL4176;mys-2(ok2429) vs CL4176]
Tight junction
Ribosome
Parkinsons disease
Oxidative phosphorylation
Notch signaling pathway
Mineral absorption
Maturity onset diabetes of the young
Malaria
Huntingtons disease
Gastric acid secretion
Galactose metabolism
Fructose and mannose metabolism
Drug metabolism – cytochrome P450
DNA replication
Cyanoamino acid metabolism
Cholinergic synapse
Basal transcription factors
Arachidonic acid metabolism
Amyotrophic lateral sclerosis (ALS)
Alzheimers disease
Pathway
RichFactor
Qvalue
Gene_number
Top 20 Statistics of Pathway Enrichment for
F1 [CL4176;mys-2 RNAi in P0 vs CL4176]
Valine, leucine and isoleucine biosynthesis
Thiamine metabolism
Pentose and glucuronate interconversions
Parkinsons disease
p53 signaling pathway
Oxidative phosphorylation
Natural killer cell mediated cytotoxicity
Metabolic pathways
Malaria
Legionellosis
Inositol phosphate metabolism
Huntingtons disease
Galactose metabolism
Fructose and mannose metabolism
Epithelial cell signaling in Helicobacter pylori infection
Arachidonic acid metabolism
Apoptosis
Amyotrophic lateral sclerosis (ALS)
Amphetamine addiction
Alzheimers disease
Pathway
RichFactor
Qvalue
Gene_number

C

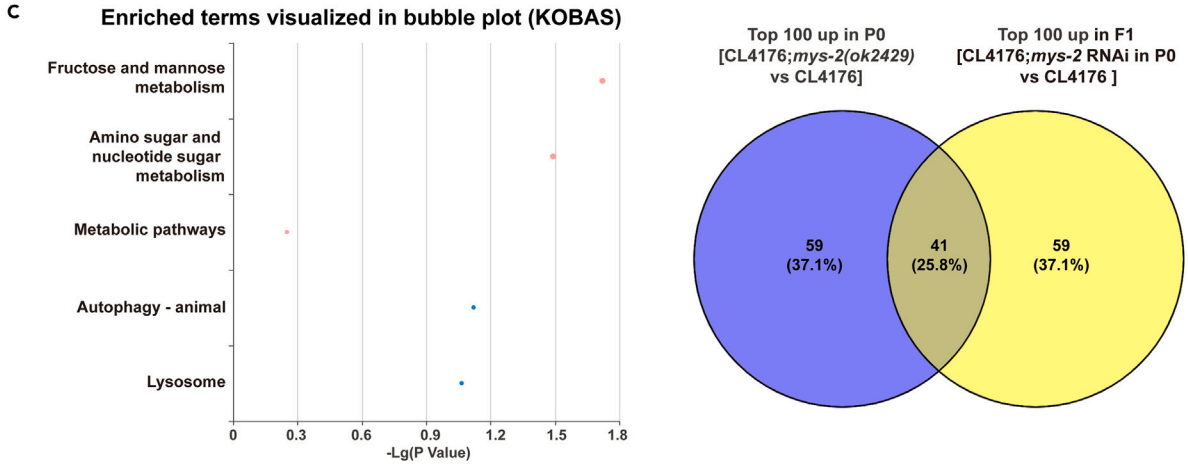
Enriched terms visualized in bubble plot (KOBAS)
Fructose and mannose metabolism
Amino sugar and nucleotide sugar metabolism
Metabolic pathways
Autophagy - animal
Lysosome
-Lg(P Value)
Top 100 up in P0 [CL4176;mys-2(ok2429) vs CL4176]
Top 100 up in F1 [CL4176;mys-2 RNAi in P0 vs CL4176]
59 (37.1%)
41 (25.8%)
59 (37.1%)

Figure 3. F1 progeny whose with the wild-type *mys-2* gene showed the similar gene expression patterns to those in the P0 generation of CL4176;*mys-2(ok2429)*

(A) Correlations of the differentially expressed genes between P0 generation (CL4176;*mys-2(ok2429)* vs. CL4176) and F1 progeny (CL4176;*mys-2* RNAi in P0 vs. CL4176) were evaluated by log10 FPKM.

(B) KEGG pathway enrichment of the differentially expressed genes in P0 generation (CL4176;*mys-2(ok2429)* vs. CL4176) (left) and F1 progeny (CL4176;*mys-2* RNAi in P0 vs. CL4176) (right). The horizontal axis represents significance of enrichment, and the longitudinal axis represents the enrichment terms. The size of each dot represents the number of genes contained in the corresponding term.

(C) Enriched terms of the top 100 upregulated genes shared by P0 and F1 visualized in a bubble plot.

sequences upstream of transcriptional start sites using the University of California at Santa Cruz (UCSC) website. The motifs identified by a motif discovery website (RSAT) as potential targets of MYS-2 included the following: CAAAAA (with e-value of 2e-44), TAAATA (1e-300), and AAATTG (4.7e-36) among the downregulated genes; and CTGAAA (3.5e-38), AAATTA (1.8e-12), and ATTTTTA (8.9e-09) among the upregulated genes. Using ChIP-qPCR, the candidate genes involved in AD-like pathophysiology (e.g., *acs-4*, *y48c3a.5*, *h14e04.2*, and *glh-2*) that were downregulated, and the upregulated genes associated with lysosome (e.g., *lys-4*, *lys-5*, *lys-6*, *lys-10*, and *ilys-3*) were chosen for analysis of enriched motifs. One or more fragments containing the target motifs in the promoter region were selected for ChIP-qPCR assay. Compared to the control CL4176 nematodes, similarly reduced levels of H4 acetylation within motifs of downregulated genes (AD-like pathophysiology) were detected in both CL4176;*mys-2* RNAi and their F1 progeny (Figure 4C), and higher levels of H4 acetylation were observed in motifs of upregulated genes (lysozymes related genes) (Figure 4D). However, the opposite changes can be observed in the comparison of CL4176 with its negative control CL802 (Figure S7), proving that those genes were not only regulated by *mys-2* but also involved in AD.

Increased lysosomal expression resulting from *mys-2* deficiency ameliorated intergenerational Aβ accumulation

To further investigate the potential reasons mechanisms by which *mys-2* deficiency improved AD pathogenesis, we used multiple techniques to monitor Aβ accumulation. Using the CL2331 strain, which expresses GFP fused to Aβ after a temperature shift from 16°C to 25°C, we compared Aβ accumulation in the presence or absence of *mys-2* mutation. The results showed that control CL2331 nematodes had significantly stronger GFP fluorescence than CL2331;*mys-2(ok2429)* nematodes (Figure 5A). In addition, the double-transgenic germline, CL4176;*mys-2(ok2429)*, was analyzed using ELISA or stained with thioflavin-T, a beta-amyloid dye that binds to amyloid fibrils. ELISA also supported that mutation of *mys-2* in either the P0 or F1 generation resulted in reduced Aβ accumulation (Figure 5B). In addition, Thioflavin-T staining showed the presence of amyloid aggregates in CL4176 nematodes, but not in CL4176;*mys-2(ok2429)* nematodes (Figure 5C). These findings suggested that reduced Aβ accumulation in either the P0 or F1 generation could be responsible for improvement of disease phenotypes.

Impairment of the autophagy-lysosomal pathway has been shown to contribute to Aβ accumulation. Our analyses of the candidate target genes also suggested that lysosomes functioned downstream of *mys-2*. Next, we observed changes in lysosomes using the fluorescent dye, LysoTracker red. Comparison of fluorescence of lysosomes in untreated CL4176 nematodes, CL4176;*mys-2(ok2429)* nematodes, and CL4176 nematodes treated with the histone acetyltransferase inhibitor MG149 showed that deficiency of *mys-2* significantly increased the number of lysosomes (Figure 5D). Similarly, lysosome numbers were also increased in the F1 progeny (Figure 5E).

The mammalian homolog MOF had a similar function as MYS-2 in AD pathogenesis

To further verify whether MOF, the mammalian homolog of MYS-2, played a similar role to MYS-2 in AD, we analyzed data from patients with AD from Alzdata: http://www.alzdata.org/index.html, and the results showed that the expression of MOF increased significantly in the frontal cortex of patients with AD (Figure 6A). Next, the effects of the *mof* gene were determined again in an AD cell model. 3-(4,5-dimethylthiazol-2-yl)-2,5-diphenyltetrazolium bromide (MTT) assay showed that cell death caused by amyloid was partially rescued by knockdown of *mof* (Figure 6B), which was consistent with the results of knockdown of *mys-2* in our *C. elegans* AD model.

Next, the interrelationships among Aβ, H4K16ac, and MOF were evaluated in AD cell models. Addition of Aβ1–42 to SH-SY5Y cells increased MOF and H4K16ac. In contrast, MOF knockdown or inactivation of MOF using MG149 suppressed H4K16ac levels in AD cell models (Figures 6C and 6D). In addition, increased lysosome formation was observed in cells with reduced MOF levels (Figure 6E).

To identify mammalian MOF target genes, ChIP-sequencing (ChIP-seq) using anti-MOF was performed in AD cell model SH-SY5Y. The DNA fragments immunoprecipitated by MOF were mapped to the entire genome background (Figure S8). Analysis using KEGG and KOBAS ontology annotation to total MOF-binding genes (fold enrichment of $\geq$200 and p values $\leq$0.01) showed that biological functions such as fructose and mannose metabolism, fatty acid biosynthesis, and lysosome were enriched (Figure 6F), consistent with the RNA-seq and ChIP-qPCR analyses of *C. elegans*. Analysis of total genes or individual genes with fold enrichment of $\geq$4 and p value $\leq$ 0.01 showed that the enriched pathways were associated with neurodegenerative diseases such as AD, PD, and HD (Figure 6G). A motif is a characteristic conserved sequence that mediates DNA binding to a protein. We therefore searched for mammalian motifs within the MOF-associated enriched genes using hypergeometric optimization of motif enrichment (HOMER)[52] using a p value cutoff for each motif match of $\leq$0.01. The common motifs from ChIP-seq analysis of SH-SY5Y cells included CACACACACA, AATAAA, ATAAAA, TTTAATG, and CCAAAAA, which were similar to the motifs of downregulated genes in *C. elegans* from ChIP-qPCR (Figure 6H), indicating that mammalian MOF and *C. elegans* MYS-2 may be functionally conserved.

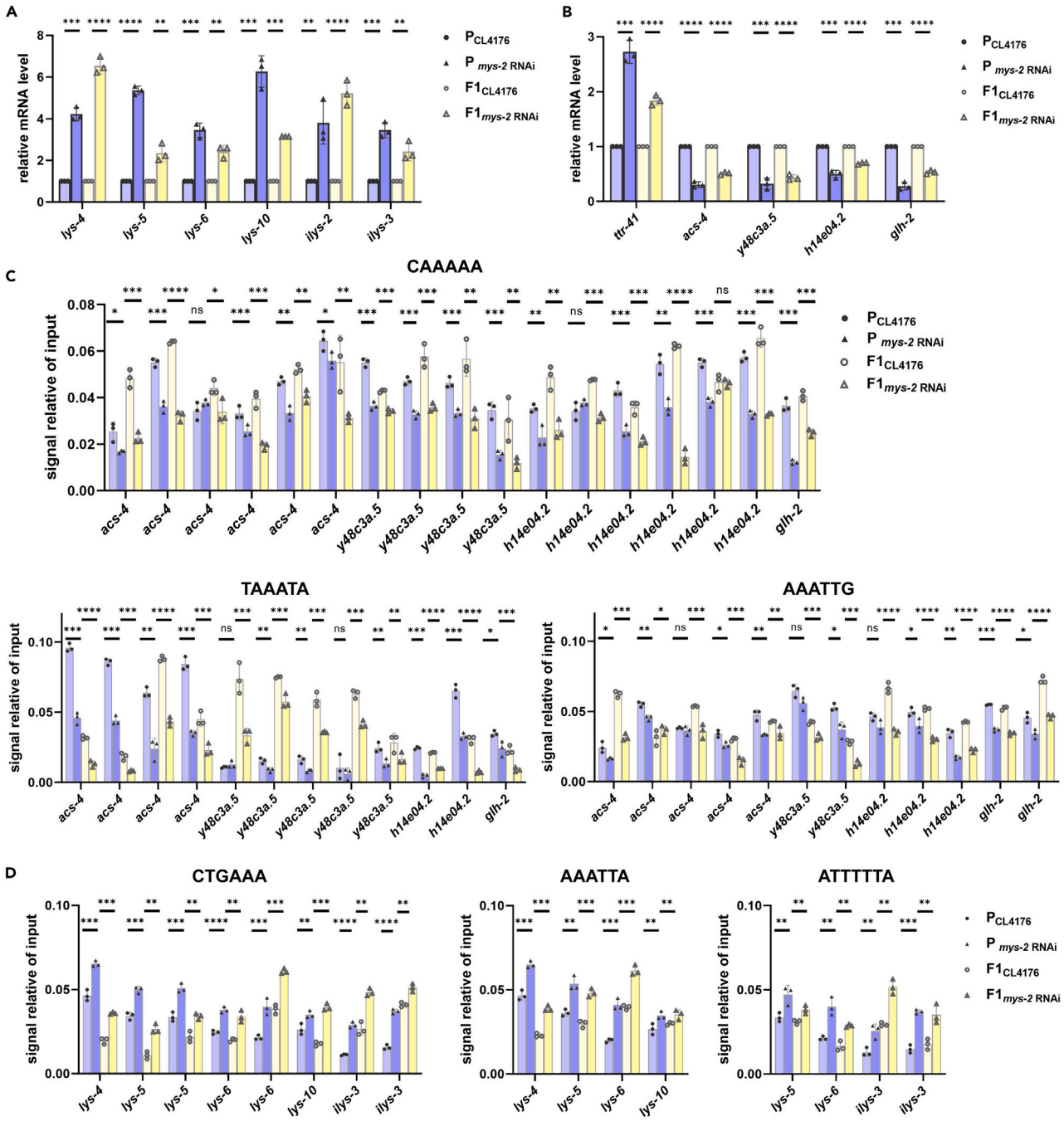

Figure 4. Similar expression levels of several genes involved in AD pathogenesis and lysozymes were observed between the P0 generation and F1 progeny

(A and B) Quantitative PCR was used to determine the expression levels of candidate genes enriched in AD-like pathophysiology (A) and lysozymes (B).

(C and D) ChIP-qPCR analysis of enriched DNA motifs within the promoter regions of the potential target genes of *mys-2*, including downregulated AD-related genes (C) and upregulated lysozyme genes (D) identified from our transcriptomic analysis. Three independent experiments were analyzed using Multiple unpaired t tests.

The ROS/CDK-5/ATM pathway was an upstream regulator of *mys-2* in AD models

Previous studies showed that MOF was regulated by ataxia telangiectasia mutated (ATM)[42,53] and that cyclin-dependent kinase-5 (CDK-5) directly phosphorylated ATM at serine 794 following DNA damage.[54,55] Furthermore, increased reactive oxygen species (ROS)in AD has

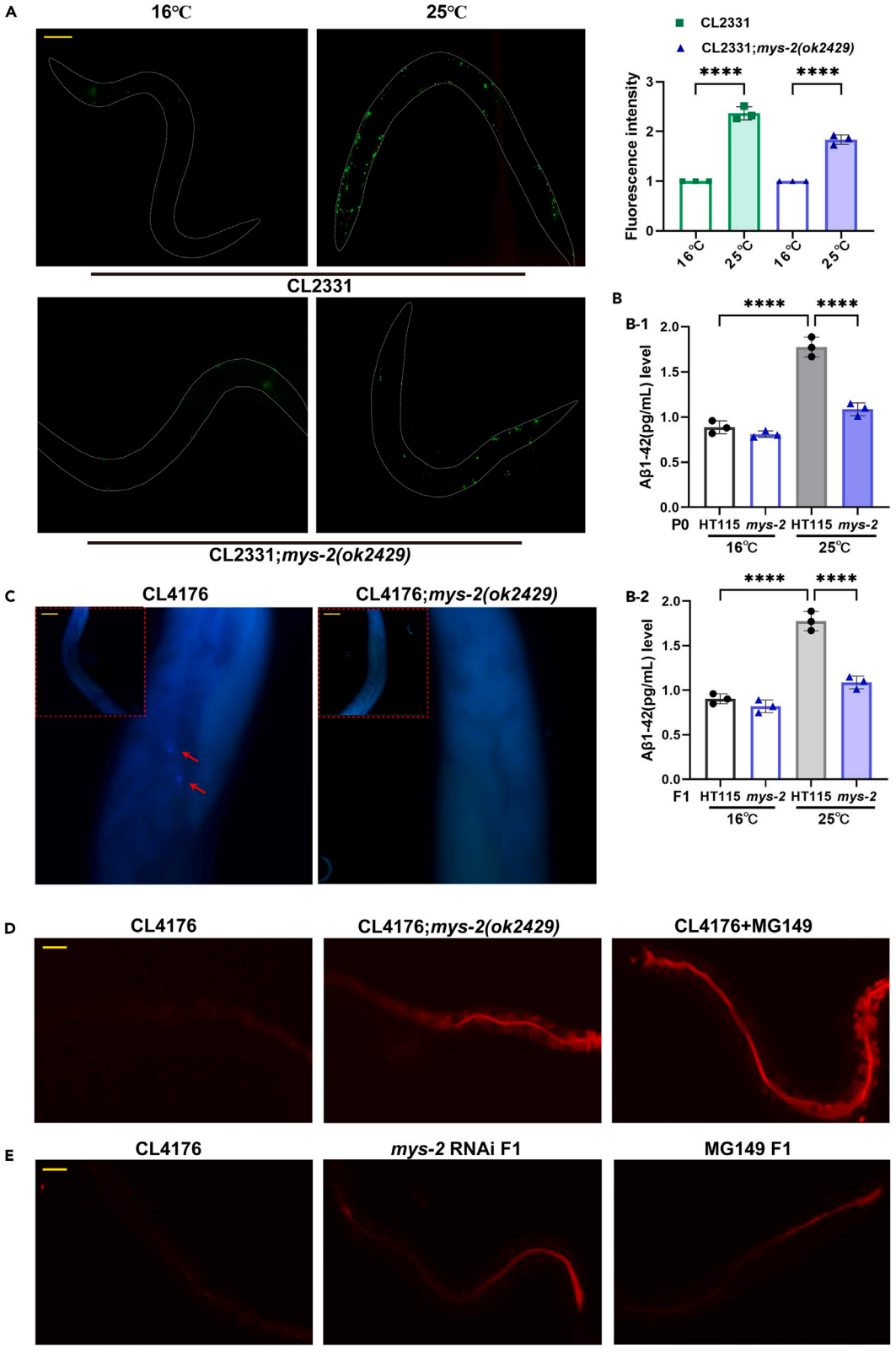
A
16℃
25℃
CL2331
CL2331;mys-2(ok2429)
CL2331
CL2331;mys-2(ok2429)
Fluorescence intensity
****
****
16℃
25℃
16℃
25℃
B
B-1
Aβ1-42(pg/mL) level
P0
HT115
mys-2
HT115
mys-2
16℃
25℃
B-2
F1
C
CL4176
CL4176;mys-2(ok2429)
D
CL4176
CL4176;mys-2(ok2429)
CL4176+MG149
E
CL4176
mys-2 RNAi F1
MG149 F1

Figure 5. The *mys-2* gene contributed to AD pathogenesis by mediating intergenerational Aβ accumulation in transgenic *C. elegans* CL4176

(A) Green fluorescence protein assay of Aβ accumulation in CL2331 nematodes and CL2331;*mys-2(ok2429)* nematodes. The bar graph showed the relative fluorescence intensity of 3 independent experiments.

(B) Accumulation of Aβ was evaluated using ELISA in P0 CL4176, CL4176;*mys-2(ok2429)*, and the F1 generation at either 16°C or 25°C.

(C) Accumulated Aβ was stained with Thioflavin-T in CL4176 and CL4176;*mys-2(ok2429)* transgenic nematodes. The red arrows indicate Aβ accumulation in the muscle of the body wall.

(D) Representative lysosomal images of CL4176, CL4176;*mys-2(ok2429)*, and CL4176+MG149. Deficiency of the putative histone acetyltransferase MYS-2 resulted in increased number of lysosomes. The lysosomes were stained with the fluorescent dye, LysoTracker red.

(E) The F1 generation also showed increased number of lysosomes. Scale bar, 50 μm.

been shown to induce oxidative damage of nucleic acids.[56,57] These findings suggested a potential signaling pathway for regulation of *mys-2* (Figure 7A).

To test the hypothesis that the ROS/CDK-5/ATM signaling pathway participated in *mys-2*-mediated AD pathogenesis, the paralytic phenotypes were assessed as a function of perturbations of components within this signaling pathway, including treatment with *cdk-5* RNAi, uric acid (an endogenous antioxidant ROS scavenger, 2 mM), or AZD0156 (an ATM inhibitor, 0.58 nM). All the drugs had no effects on chromatins, DNAs or RNAs been reported. The results showed that each of these treatments delayed paralysis similar to the delay observed in response to *mys-2* RNAi. These results indicated that all components of the ROS/CDK-5/ATM contributed to AD pathogenesis in our model (Figure 7B). To further determine whether these genes function within the same pathway, we assayed their cumulative effects among various genes. We found that the ATM inhibitor AZD0156, combined with *cdk-5* RNAi and a double RNAi targeting *cdk-5* and *mys-2* produced paralysis comparable to that observed with *ckd-5* RNAi, *mys-2* RNAi, or AZD0156 alone (Figure 7C). These results suggested that ROS, CDK-5, ATM, and MYS-2 functioned within the same pathway in AD pathogenesis. Furthermore, dominant phenotypes of the corresponding downstream genes in this signaling pathway were also observed in response to combined RNAi knockdown of *mys-2* and *cdk-5*, uric acid (for scavenging ROS), or chloroquine diphosphate (CHQ) (an activator of ATM, 1 μM). For example, in combination with CHQ, *mys-2* RNAi produced a similar phenotype to that produced by *mys-2* RNAi alone. Furthermore, combinations of uric acid and CHQ or *cdk-5* RNAi and CHQ recapitulated the phenotype resulting from ATM activation (Figure 7D). We further investigated the effects of components of the ROS/CDK-5/ATM pathway on lysosomal production. Downregulation of each component in this pathway enhanced lysosomal production, with dominant phenotypes of the corresponding downstream genes also observed (Figure 7E). Finally, we confirmed that the ROS/CDK-5/ATM signaling pathway affected acetylation levels of H4K16 as a pathway upstream of MYST acetyltransferase. Treatment with uric acid (for scavenging ROS), or roscovitine (inhibitor of CDK-5, 0.5 μM), AZD0156 (0.58 nM), or MG149 (50 μM) to inhibit CDK-5, ATM, or MOF, respectively, resulted in decreased H4K16ac levels (Figure 7F).

To evaluate the role of the ROS/CDK-5/ATM signaling pathway in intergenerational epigenetic inheritance, ADZ0156 was added to the P0 generation and then a series of phenotypes such as the paralysis rates, lysosomal activity, and H4K16ac levels were analyzed in F1 progeny. As expected, inactivation of the ROS/CDK-5/ATM signaling pathway in the P0 generation resulted in delayed paralysis (Figure 7G), enhanced lysosome activity (Figure 7H), and decreased H4K16ac (Figure 7I) in the F1 generation. Moreover, in mammalian cells, the ROS/CDK-5/ATM pathway was also shown to function upstream of MOF and to regulate MOF-mediated AD pathogenesis (Figures S9A and S9B), lysosome formation (Figures S9C and S9D), and H4K16ac too (Figure S9E), indicating it was a conserved manner that ROS/CDK-5/ATM signaling pathway regulated MYS-2/MOF and the related biological processes.

DISCUSSION

In contrast to irreversible genetic mutations, epigenetic changes can be manipulated or corrected through classical pharmacology. Drugs targeting DNA methylation and histone modification have shown therapeutic benefit in cancer and neuropsychiatric disorders.[58,59] Inhibition of HAT activity and use of HDAC activators are potential therapeutic approaches for slowing or halting progression of dementia in AD.[17] However, further the underlying mechanisms or potential targets of candidate drugs have not been identified.

Being a key modification that controls chromatin compression and gene expression, H4K16ac has been shown to be altered in patients with AD who had an overall decrease in the total number of H4K16ac peaks compared to the normal elderly.[12] The *mys-2* gene encodes an MYST acetyltransferase that is orthologous to *Drosophila* CG1894, the human MOF protein, and the *Saccharomyces cerevisiae* SAS2 protein. In mammalian cells, the ortholog of MOF/KAT8 (lysine acetyltransferase 8) forms two different protein complexes: the male-specific lethal (MSL) complex and the nonspecific lethal (NSL) complex, both of which acetylate histone H4 at lysine 16 (H4K16).[60,61] Although few studies have established a direct correlation between MOF and AD, MOF has been shown to regulate a series of cellular processes/pathways that significantly contribute to the etiology of AD, such as ROS accumulation, mitochondrial dysfunction, deleterious effects on biomolecules (e.g., proteins, DNA/RNA, and lipids) during oxygen-respiratory stress, and apoptosis/necrosis of neurons.[62,63] In the present study, MYS-2 exerted similar acetyltransferase activity at H4K16 as that of human MOF/KAT8, both of which positively regulated a number of genes associated with known AD-related pathways, as demonstrated by ChIP-PCR and transcriptomic analyses. Increased lysosome activity in *mys-2* knockdown or knockout mutant removed Aβ build-up and alleviated AD pathogenesis. In patients with AD, Aβ has been shown to impair lysosomal function via de-acidification and membrane permeabilization. The expression levels of lysosomal proteins such as LAMP1 (lysosome-associated membrane protein 1) and LAMP2, which are markers of lysosomal function, have been shown to change in response to Aβ deposition or with onset of AD.[64,65] In our study, *C. elegans mys-2* modulated lysosomal gene transcription, similar to that observed in a previous high throughput analysis of MOF in a mammalian model.[66]

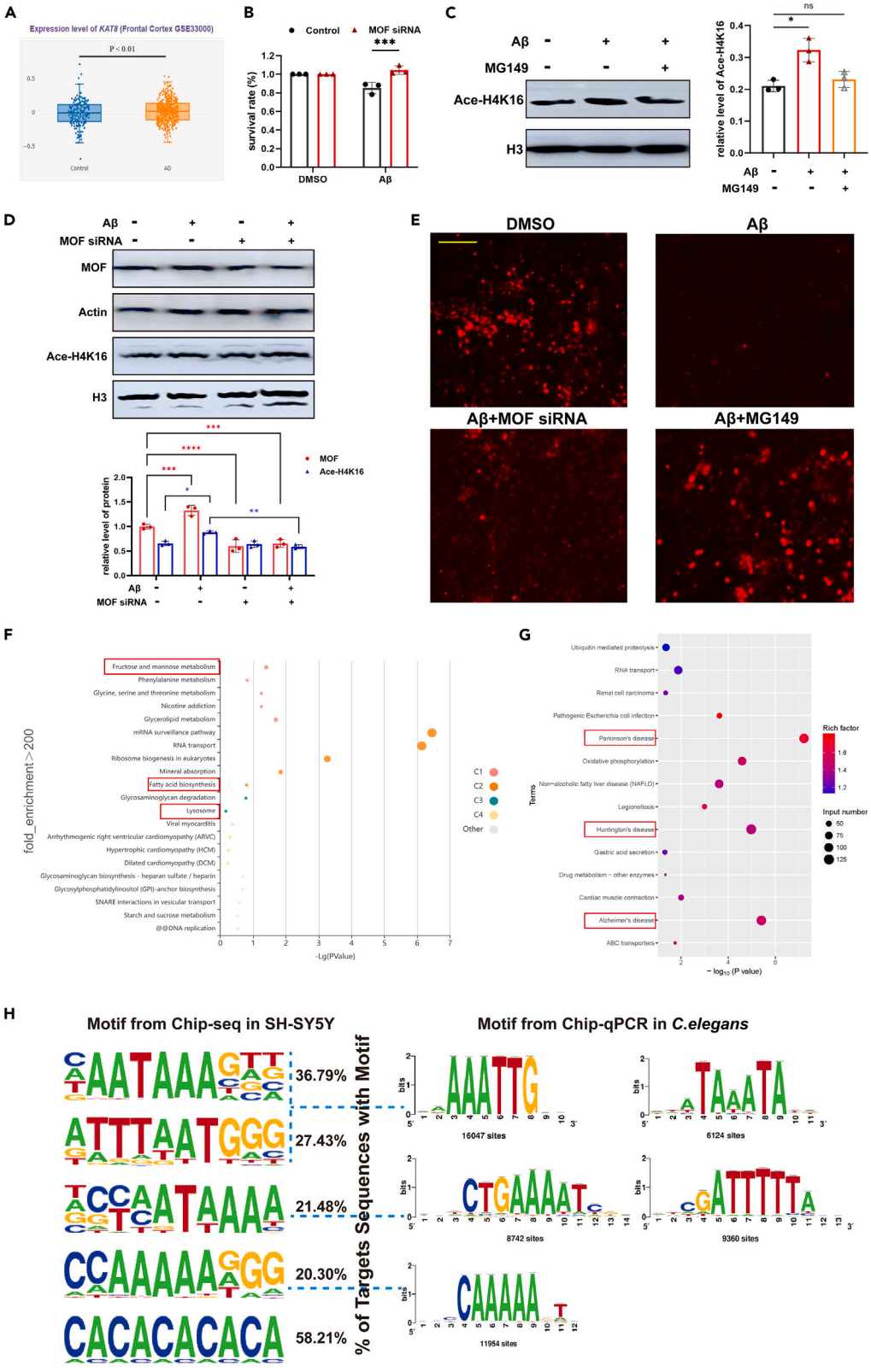
A
Expression level of KAT8 (Frontal Cortex GSE33000)
P < 0.01
Control
AD
B
Control
MOF siRNA
***
survival rate (%)
DMSO
Aβ
C
Aβ
MG149
Ace-H4K16
H3
ns
*
relative level of Ace-H4K16
D
Aβ
MOF siRNA
MOF
Actin
Ace-H4K16
H3
MOF
Ace-H4K16
relative level of protein
E
DMSO
Aβ
Aβ+MOF siRNA
Aβ+MG149
F
Fructose and mannose metabolism
Phenylalanine metabolism
Glycine, serine and threonine metabolism
Nicotine addiction
Glycerolipid metabolism
mRNA surveillance pathway
RNA transport
Ribosome biogenesis in eukaryotes
Mineral absorption
Fatty acid biosynthesis
Glycosaminoglycan degradation
Lysosome
Viral myocarditis
Arrhythmogenic right ventricular cardiomyopathy (ARVC)
Hypertrophic cardiomyopathy (HCM)
Dilated cardiomyopathy (DCM)
Glycosaminoglycan biosynthesis - heparan sulfate / heparin
Glycosylphosphatidylinositol (GPI)-anchor biosynthesis
SNARE interactions in vesicular transport
Starch and sucrose metabolism
@@DNA replication
fold_enrichment>200
-Lg(PValue)
C1
C2
C3
C4
Other
G
Ubiquitin mediated proteolysis
RNA transport
Renal cell carcinoma
Pathogenic Escherichia coli infection
Parkinson's disease
Oxidative phosphorylation
Non-alcoholic fatty liver disease (NAFLD)
Legionellosis
Huntington's disease
Gastric acid secretion
Drug metabolism - other enzymes
Cardiac muscle contraction
Alzheimer's disease
ABC transporters
Terms
Rich factor
Input number
50
75
100
125
− log10 (P value)
H
Motif from Chip-seq in SH-SY5Y
Motif from Chip-qPCR in C.elegans
36.79%
27.43%
21.48%
20.30%
58.21%
% of Targets Sequences with Motif
16047 sites
6124 sites
8742 sites
9360 sites
11954 sites
bits

Figure 6. The mammalian homolog of MYS-2, MOF, participated in AD pathogenesis in a mammalian cell model of AD

(A) Analysis of mammalian MOF(KAT8) in the frontal cortex of patients with AD. The data of MOF expression from Alzdata (http://www.alzdata.org/index.html). Data number: GSE33000.

(B) Cell survival analysis using MTT assay in SH-SY5Y cells following treatment with 100 nM Aβ1–42 showed that MOF siRNA increased cellular resistance to Aβ.

(C) Western blotting of H4K16ac in an AD model of SH-SY5Y cell.

(D) In the AD model of SH-SY5Y, addition of Aβ1–42 increased MOF and H4K16ac levels, whereas MOF siRNA reduced H4K16 acetylation.

(E) Lysosomal activities were restored after inhibition of *mys-2* by adding MG149 in Aβ1–42 SH-SY5Y cells. Scale bar 200 μm.

(F) Enriched terms of MOF-binding gene targets via ChIP-seq in an AD model of SH-SY5Y cell. Bubble plot using KOBAS (fold enrichment $\geq$200 and *p* value was $\leq$0.001).

(G) KEGG pathway enrichment of MOF-binding genes (fold enrichment $\geq$4, *p*-value was $\leq$0.01). The horizontal axis represents the significance of enrichment, and the longitudinal axis represents the enrichment terms. The size of each dot represents the number of genes contained in the corresponding term.

(H) Common motifs of MOF obtained from ChIP-seq data from SH-SY5Y cell and ChIP-qPCR from *C. elegans*.

Studies of epigenetic inheritance have increased recently and have been used to explain transgenerational phenotypes in animals that could not be explained by DNA mutation or Mendelian genetics. Transgenerational effects occur in a number of disparate phenotypes, including heat stress responses and eye color in *Drosophila*,[67,68] reproduction and longevity in *C. elegans*,[27,69] cellular metabolism in Sprague-Dawley rats,[70] and the complex neuronal behaviors in learning[29,30] or drug addiction.[71] Moreover, abnormal epigenetics has been directly linked to human disease. For example, the chromosomal methylation states of the MLH1 and MSH2 alleles have been shown to persist to two or three successive generations in families with hereditary nonpolyposis colorectal cancer, providing the most convincing example of transgenerational inheritance of epigenetics.[72,73] The epigenetic factors responsible for transgenerational phenotypic or disease heritability encompass small non-coding RNAs (sncRNAs), DNA methylation, and histone modifications.[74,75] A recent study suggested that H4K16ac catalyzed by MOF can be maintained from oocytes to fertilized embryos in Drosophila and mammals, which modulated the nucleosome accessibility prior to transcriptional activation of MOF and primed the future gene activation required in early embryogenesis of offspring.[35] Our current results also support intergenerational heritability of H4K16 and the reprogrammed gene expression across generations that contributes for AD development in the offspring of *C. elegans*.

Limitations of the study

Overall, we here have suggested a role for MYS-2/MOF in AD pathogenesis and intergenerational transmission of epigenetic modifications in familial clustering AD. Although transgene models *C. elegans* have widely reported in Alzheimer's disease and many neurodegenerative diseases researches,[37,76] the samples from AD patients should be used in future studies to verify the intergenerational inheritance and the potential mechanism.

STAR★METHODS

Detailed methods are provided in the online version of this paper and include the following:

- KEY RESOURCES TABLE
- RESOURCE AVAILABILITY
  - Lead contact
  - Materials availability
  - Data and code availability
- EXPERIMENTAL MODEL AND STUDY PARTICIPANT DETAILS
  - *C. elegans* strain and culture
  - Cell line
- METHOD DETAILS
  - Paralysis assay
  - RNAi protocol
  - Staining of Aβ and lysosome
  - ELISA analysis of Aβ
  - Western blotting
  - RNA-seq
  - Chromatin-immunoprecipitation sequencing (ChIP-seq) and ChIP–quantitative polymerase chain reaction (ChIP-qPCR)
  - Localization of *mys-2* expression
- QUANTIFICATION AND STATISTICAL ANALYSIS

SUPPLEMENTAL INFORMATION

Supplemental information can be found online at https://doi.org/10.1016/j.isci.2024.110588.

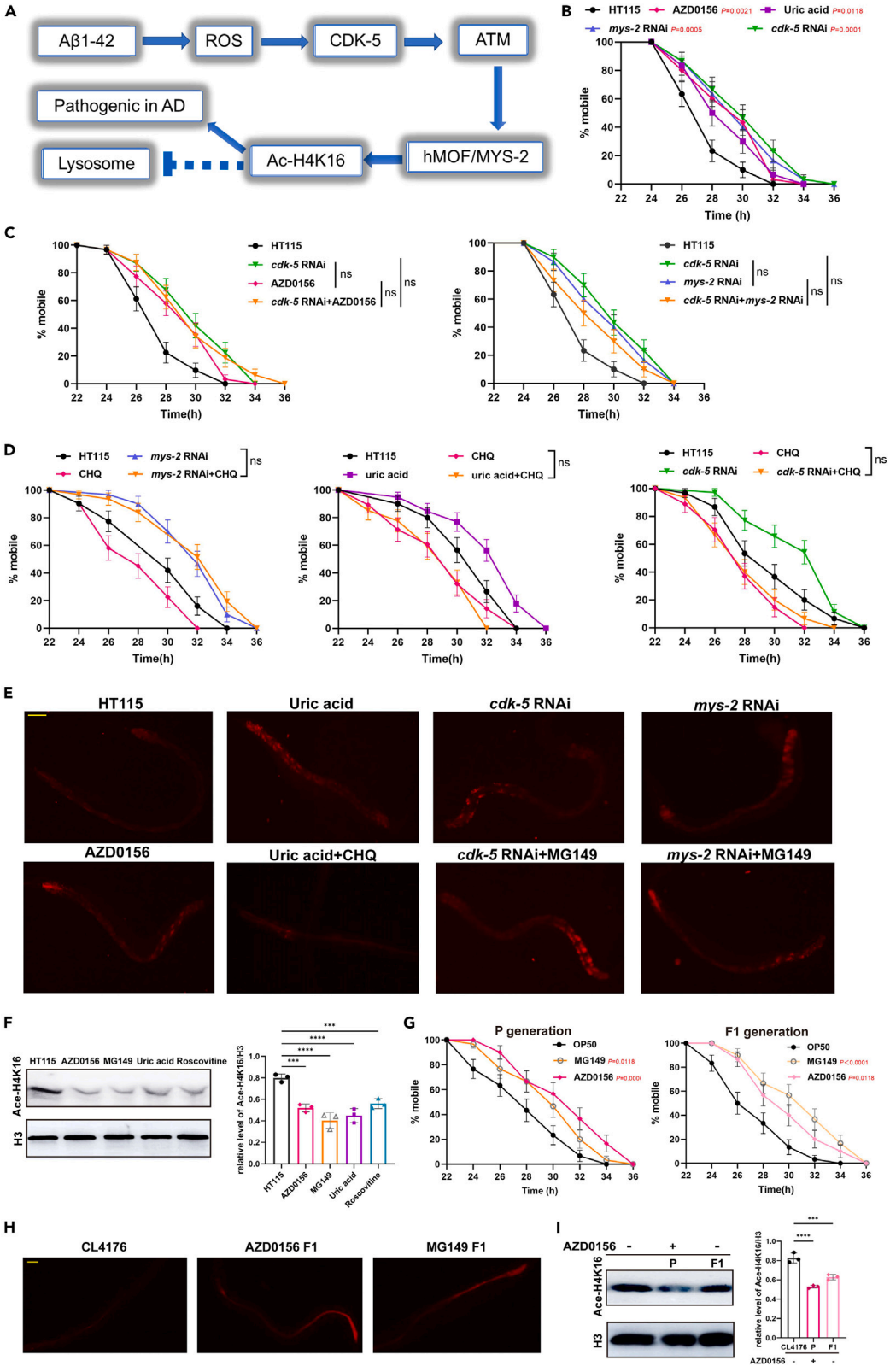
A
Aβ1-42
ROS
CDK-5
ATM
Pathogenic in AD
Lysosome
Ac-H4K16
hMOF/MYS-2
B
HT115
AZD0156 P=0.0021
Uric acid P=0.0118
mys-2 RNAi P=0.0005
cdk-5 RNAi P=0.0001
% mobile
Time (h)
C
HT115
cdk-5 RNAi
AZD0156
cdk-5 RNAi+AZD0156
mys-2 RNAi
cdk-5 RNAi+mys-2 RNAi
ns
% mobile
Time(h)
D
HT115
mys-2 RNAi
CHQ
mys-2 RNAi+CHQ
uric acid
uric acid+CHQ
cdk-5 RNAi
cdk-5 RNAi+CHQ
E
HT115
Uric acid
cdk-5 RNAi
mys-2 RNAi
AZD0156
Uric acid+CHQ
cdk-5 RNAi+MG149
mys-2 RNAi+MG149
F
HT115 AZD0156 MG149 Uric acid Roscovitine
Ace-H4K16
H3
relative level of Ace-H4K16/H3
G
P generation
F1 generation
OP50
MG149 P=0.0118
AZD0156 P=0.0001
MG149 P<0.0001
AZD0156 P=0.0118
% mobile
Time (h)
Time(h)
H
CL4176
AZD0156 F1
MG149 F1
I
AZD0156
P
F1
Ace-H4K16
H3
relative level of Ace-H4K16/H3
CL4176

Figure 7. ROS/CDK-5/ATM functioned upstream of *mys-2* and modulated H4K16ac in both the P and F1 generations

(A) Proposed signaling pathway for regulation of MYS-2 in *C. elegans*. *p* value presented as the comparison with HT115.

(B) Functional validation of key genes within the ROS/CDK-5/ATM/MYS-2 signaling pathway suggested a similar role for AD-like pathogenesis for each component within the signaling pathway.

(C) No cumulative effects were observed among the various genes or ATM inhibitor.

(D) The dominant phenotypes of downstream genes within the ROS/CDK-5/ATM signaling pathway.

(E) Lysosomal staining to assess changes in lysosomal activities among the various treatment groups, including uric acid for scavenging ROS, an ATM inhibitor (AZD0156), an ATM activator (CHQ), and RNAi.

(F) Western blotting and quantification to determine H4K16ac levels in CL4176 nematodes after addition of inhibitors (roscovitine for CDK-5, AZD0156 for ATM, and MG149 for MOF), and uric acid for scavenging ROS.

(G) F1 progeny whose parents had been treated with MG149 and AZD0156 showed delayed paralysis. *p* value presented as the comparison with OP50.

(H) Increased numbers of lysosomes were observed in the F1 progeny whose parents had been treated with MG149 and AZD0156.

(I) Western blotting of H4K16ac in CL4176 nematodes and CL4176 nematodes treated with AZD0156 in the P0 generation and F1 progeny. Scale bar, 50 μm.

ACKNOWLEDGMENTS

This work was supported by the National Natural Science Foundation Program of China (grant no. 32170184), and Yunnan Fundamental Research Projects (grant nos. 202201AT070233, 202403AC100007).

Committee approval: The Academic Committee of Yunnan University approved the experiments and confirm that all experiments comply with the relevant regulatory standards.

AUTHOR CONTRIBUTIONS

Y.H. Li, H.Bai, W.W. Liu, W.H. Zhou, H.GuP.J.Zhao, M.Zhu, Y.X. Li, and X.Y. Yan conducted the experiments and analyzed the data; X.W. Huang and N.H. Zhao signed the experiments and supported the funding; X.W. Huang, Y.H. Li. and H. Bai wrote the paper. All authors have read and approved the final manuscript.

DECLARATION OF INTERESTS

The authors declare no competing interests.

Received: July 1, 2023
Revised: February 8, 2024
Accepted: July 23, 2024
Published: July 25, 2024

REFERENCES

1. Guo, H., Cao, H., Cui, X., Zheng, W., Wang, S., Yu, J., and Chen, Z. (2019). Silymarin's Inhibition and Treatment Effects for Alzheimer's Disease. Molecules *24*, 1748. https://doi.org/10.3390/molecules24091748.
2. Alzheimer's Disease International (2018). World Alzheimer Report 2018 (London, GB: ADI). https://www.alz.co.uk/research/WorldAlzheimerReport2018.pdf.
3. Cacace, R., Sleegers, K., and Van Broeckhoven, C. (2016). Molecular genetics of early-onset Alzheimer's disease revisited. Alzheimers Dement. *12*, 733–748. https://doi.org/10.1016/j.jalz.2016.01.012.
4. Zekanowski, C., Styczyńska, M., Pepłońska, B., Gabryelewicz, T., Religa, D., Ilkowski, J., Kijanowska-Haładyna, B., Kotapka-Minc, S., Mikkelsen, S., Pfeffer, A., et al. (2003). Mutations in presenilin 1, presenilin 2 and amyloid precursor protein genes in patients with early-onset Alzheimer's disease in Poland. Exp. Neurol. *184*, 991–996. https://doi.org/10.1016/S0014-4886(03)00384-4.
5. Hoogmartens, J., Cacace, R., and Van Broeckhoven, C. (2021). Insight into the genetic etiology of Alzheimer's disease: A comprehensive review of the role of rare variants. Alzheimers Dement. *13*, e12155. https://doi.org/10.1002/dad2.12155.
6. Janssen, J.C., Beck, J.A., Campbell, T.A., Dickinson, A., Fox, N.C., Harvey, R.J., Houlden, H., Rossor, M.N., and Collinge, J. (2003). Early onset familial Alzheimer's disease: Mutation frequency in 31 families. Neurology *60*, 235–239. https://doi.org/10.1212/01.wnl.0000042088.22694.e3.
7. Lleó, A., Blesa, R., Queralt, R., Ezquerra, M., Molinuevo, J.L., Peña-Casanova, J., Rojo, A., and Oliva, R. (2002). Frequency of mutations in the presenilin and amyloid precursor protein genes in early-onset Alzheimer disease in Spain. Arch. Neurol. *59*, 1759–1763. https://doi.org/10.1001/archneur.59.11.1759.
8. Yagi, R., Miyamoto, R., Morino, H., Izumi, Y., Kuramochi, M., Kurashige, T., Maruyama, H., Mizuno, N., Kurihara, H., and Kawakami, H. (2014). Detecting gene mutations in Japanese Alzheimer's patients by semiconductor sequencing. Neurobiol. Aging *35*, 1780.e1. https://doi.org/10.1016/j.neurobiolaging.2014.01.023.
9. An, S.S., Park, S.A., Bagyinszky, E., Bae, S.O., Kim, Y.J., Im, J.Y., Park, K.W., Park, K.H., Kim, E.J., Jeong, J.H., et al. (2016). A genetic screen of the mutations in the Korean patients with early-onset Alzheimer's disease. Clin. Interv. Aging *11*, 1817–1822. https://doi.org/10.2147/CIA.S116724.
10. Jia, L., Fu, Y., Shen, L., Zhang, H., Zhu, M., Qiu, Q., Wang, Q., Yan, X., Kong, C., Hao, J., et al. (2020). PSEN1, PSEN2, and APP mutations in 404 Chinese pedigrees with familial Alzheimer's disease. Alzheimers Dement. *16*, 178–191. https://doi.org/10.1002/alz.12005.
11. Sanchez-Mut, J.V., and Gräff, J. (2015). Epigenetic Alterations in Alzheimer's Disease. Front. Behav. Neurosci. *9*, 347. https://doi.org/10.3389/fnbeh.2015.00347.
12. Nativio, R., Donahue, G., Berson, A., Lan, Y., Amlie-Wolf, A., Tuzer, F., Toledo, J.B., Gosai, S.J., Gregory, B.D., Torres, C., et al. (2018). Dysregulation of the epigenetic landscape of normal aging in Alzheimer's disease. Nat. Neurosci. *21*, 497–505. https://doi.org/10.1038/s41593-018-0101-9.
13. Benayoun, B.A., Pollina, E.A., and Brunet, A. (2015). Epigenetic regulation of ageing: linking environmental inputs to genomic stability. Nat. Rev. Mol. Cell Biol. *16*, 593–610. https://doi.org/10.1038/nrm4048.
14. Baltazar, M.T., Dinis-Oliveira, R.J., de Lourdes Bastos, M., Tsatsakis, A.M., Duarte, J.A., and Carvalho, F. (2014). Pesticides exposure as etiological factors of Parkinson's disease and other neurodegenerative diseases–a mechanistic approach. Toxicol. Lett. *230*, 85–103. https://doi.org/10.1016/j.toxlet.2014.01.039.
15. Morris, M.C., and Tangney, C.C. (2014). Dietary fat composition and dementia risk. Neurobiol. Aging *35*, S59–S64. https://doi.org/10.1016/j.neurobiolaging.2014.03.038.

16. Lithner, C.U., Lacor, P.N., Zhao, W.Q., Mustafiz, T., Klein, W.L., Sweatt, J.D., and Hernandez, C.M. (2013). Disruption of neocortical histone H3 homeostasis by soluble Aβ: implications for Alzheimer's disease. Neurobiol. Aging *34*, 2081–2090. https://doi.org/10.1016/j.neurobiolaging.2012.12.028.
17. Lu, X., Wang, L., Yu, C., Yu, D., and Yu, G. (2015). Histone Acetylation Modifiers in the Pathogenesis of Alzheimer's Disease. Front. Cell. Neurosci. *9*, 226. https://doi.org/10.3389/fncel.2015.00226.
18. Lu, X., Deng, Y., Yu, D., Cao, H., Wang, L., Liu, L., Yu, C., Zhang, Y., Guo, X., and Yu, G. (2014). Histone acetyltransferase p300 mediates histone acetylation of PS1 and BACE1 in a cellular model of Alzheimer's disease. PLoS One *9*, e103067. https://doi.org/10.1371/journal.pone.0103067.
19. Kozikowski, A.P., Chen, Y., Subhasish, T., Lewin, N.E., Blumberg, P.M., Zhong, Z., D'Annibale, M.A., Wang, W.L., Shen, Y., and Langley, B. (2009). Searching for disease modifiers-PKC activation and HDAC inhibition - a dual drug approach to Alzheimer's disease that decreases Abeta production while blocking oxidative stress. ChemMedChem *4*, 1095–1105. https://doi.org/10.1002/cmdc.200900045.
20. Xu, S., and Elefant, F. (2015). Tip off the HAT-Epigenetic control of learning and memory by Drosophila Tip60. Fly *9*, 22–28. https://doi.org/10.1080/19336934.2015.1080887.
21. Julien, C., Tremblay, C., Emond, V., Lebbadi, M., Salem, N., Jr., Bennett, D.A., and Calon, F. (2009). Sirtuin 1 reduction parallels the accumulation of tau in Alzheimer disease. J. Neuropathol. Exp. Neurol. *68*, 48–58. https://doi.org/10.1097/NEN.0b013e3181922348.
22. Srivastava, S., and Haigis, M.C. (2011). Role of sirtuins and calorie restriction in neuroprotection: implications in Alzheimer's and Parkinson's diseases. Curr. Pharm. Des. *17*, 3418–3433. https://doi.org/10.2174/138161211798072526.
23. Wang, Y.J., Okutani, F., Murata, Y., Taniguchi, M., Namba, T., and Kaba, H. (2013). Histone acetylation in the olfactory bulb of young rats facilitates aversive olfactory learning and synaptic plasticity. Neuroscience *232*, 21–31. https://doi.org/10.1016/j.neuroscience.2012.12.015.
24. Peleg, S., Sananbenesi, F., Zovoilis, A., Burkhardt, S., Bahari-Javan, S., Agis-Balboa, R.C., Cota, P., Wittnam, J.L., Gogol-Doering, A., Opitz, L., et al. (2010). Altered histone acetylation is associated with age-dependent memory impairment in mice. Science (New York, N.Y.) *328*, 753–756. https://doi.org/10.1126/science.1186088.
25. Dang, W., Steffen, K.K., Perry, R., Dorsey, J.A., Johnson, F.B., Shilatifard, A., Kaeberlein, M., Kennedy, B.K., and Berger, S.L. (2009). Histone H4 lysine 16 acetylation regulates cellular lifespan. Nature *459*, 802–807. https://doi.org/10.1038/nature08085.
26. Li, C., He, X., Huang, Z., Han, L., Wu, X., Li, L., Xin, Y., Ge, J., Sha, J., Yin, Z., and Wang, Q. (2020). Melatonin ameliorates the advanced maternal age-associated meiotic defects in oocytes through the SIRT2-dependent H4K16 deacetylation pathway. Aging *12*, 1610–1623. https://doi.org/10.18632/aging.102703.
27. Greer, E.L., Maures, T.J., Ucar, D., Hauswirth, A.G., Mancini, E., Lim, J.P., Benayoun, B.A., Shi, Y., and Brunet, A. (2011). Transgenerational epigenetic inheritance of longevity in Caenorhabditis elegans. Nature *479*, 365–371. https://doi.org/10.1038/nature10572.
28. Ma, C., Niu, R., Huang, T., Shao, L.W., Peng, Y., Ding, W., Wang, Y., Jia, G., He, C., Li, C.Y., et al. (2019). N6-methyldeoxyadenine is a transgenerational epigenetic signal for mitochondrial stress adaptation. Nat. Cell Biol. *21*, 319–327. https://doi.org/10.1038/s41556-018-0238-5.
29. Moore, R.S., Kaletsky, R., and Murphy, C.T. (2019). Piwi/PRG-1 Argonaute and TGF-β Mediate Transgenerational Learned Pathogenic Avoidance. Cell *177*, 1827–1841.e12. https://doi.org/10.1016/j.cell.2019.05.024.
30. Kaletsky, R., Moore, R.S., Vrla, G.D., Parsons, L.R., Gitai, Z., and Murphy, C.T. (2020). C. elegans interprets bacterial non-coding RNAs to learn pathogenic avoidance. Nature *586*, 445–451. https://doi.org/10.1038/s41586-020-2699-5.
31. Kelly, W.G. (2014). Transgenerational epigenetics in the germline cycle of Caenorhabditis elegans. Epigenet. Chromatin *7*, 6. https://doi.org/10.1186/1756-8935-7-6.
32. Wu, Y., and Luo, Y. (2005). Transgenic C. elegans as a model in Alzheimer's research. Curr. Alzheimer Res. *2*, 37–45. https://doi.org/10.2174/1567205052772768.
33. Fang, E.F., Hou, Y., Palikaras, K., Adriaanse, B.A., Kerr, J.S., Yang, B., Lautrup, S., Hasan-Olive, M.M., Caponio, D., Dan, X., et al. (2019). Mitophagy inhibits amyloid-β and tau pathology and reverses cognitive deficits in models of Alzheimer's disease. Nat. Neurosci. *22*, 401–412. https://doi.org/10.1038/s41593-018-0332-9.
34. Cui, W.B., Zhang, Z.P., Bai, X., Wang, S.S., Chen, X.H., Liu, X., Su, P.J., Zhi, D.J., Fei, D.Q., Zhang, Z.X., and Wang, D.S. (2022). Cryptotanshinone Alleviates Oxidative Stress and Reduces the Level of Abnormally Aggregated Protein in *Caenorhabditis elegans* AD Models. Int. J. Mol. Sci. *23*, 10030. https://doi.org/10.3390/ijms231710030.
35. Samata, M., Alexiadis, A., Richard, G., Georgiev, P., Nuebler, J., Kulkarni, T., Renschler, G., Basilicata, M.F., Zenk, F.L., Shvedunova, M., et al. (2020). Intergenerationally Maintained Histone H4 Lysine 16 Acetylation Is Instructive for Future Gene Activation. Cell *182*, 127–144.e23. https://doi.org/10.1016/j.cell.2020.05.026.
36. Harris, T.W., Chen, N., Cunningham, F., Tello-Ruiz, M., Antoshechkin, I., Bastiani, C., Bieri, T., Blasiar, D., Bradnam, K., Chan, J., et al. (2004). WormBase: a multi-species resource for nematode biology and genomics. Nucleic Acids Res. *32*, D411–D417. https://doi.org/10.1093/nar/gkh066.
37. Alexander, A.G., Marfil, V., and Li, C. (2014). Use of Caenorhabditis elegans as a model to study Alzheimer's disease and other neurodegenerative diseases. Front. Genet. *5*, 279. https://doi.org/10.3389/fgene.2014.00279.
38. Dostal, V., and Link, C.D. (2010). Assaying β-amyloid toxicity using a transgenic C. elegans model. J. Vis. Exp. *44*, 2252. https://doi.org/10.3791/2252.
39. Ghizzoni, M., Wu, J., Gao, T., Haisma, H.J., Dekker, F.J., and George Zheng, Y. (2012). 6-alkylsalicylates are selective Tip60 inhibitors and target the acetyl-CoA binding site. Eur. J. Med. Chem. *47*, 337–344. https://doi.org/10.1016/j.ejmech.2011.11.001.
40. Yücel, D., Hoe, M., Llamosas, E., Kant, S., Jamieson, C., Young, P.A., Crossley, M., and Nicholas, H.R. (2014). SUMV-1 antagonizes the activity of synthetic multivulva genes in Caenorhabditis elegans. Dev. Biol. *392*, 266–282. https://doi.org/10.1016/j.ydbio.2014.05.018.
41. Füllgrabe, J., Lynch-Day, M.A., Heldring, N., Li, W., Struijk, R.B., Ma, Q., Hermanson, O., Rosenfeld, M.G., Klionsky, D.J., and Joseph, B. (2013). The histone H4 lysine 16 acetyltransferase hMOF regulates the outcome of autophagy. Nature *500*, 468–471. https://doi.org/10.1038/nature12313.
42. Zhong, J., Ji, L., Chen, H., Li, X., Zhang, J., Wang, X., Wu, W., Xu, Y., Huang, F., Cai, W., and Sun, Z.S. (2017). Acetylation of hMOF Modulates H4K16ac to Regulate DNA Repair Genes in Response to Oxidative Stress. Int. J. Biol. Sci. *13*, 923–934. https://doi.org/10.7150/ijbs.17260.
43. Marré, J., Traver, E.C., and Jose, A.M. (2016). Extracellular RNA is transported from one generation to the next in Caenorhabditis elegans. Proc. Natl. Acad. Sci. USA *113*, 12496–12501. https://doi.org/10.1073/pnas.1608959113.
44. Kim, T.W., Pettingell, W.H., Jung, Y.K., Kovacs, D.M., and Tanzi, R.E. (1997). Alternative cleavage of Alzheimer-associated presenilins during apoptosis by a caspase-3 family protease. Science (New York, N.Y.) *277*, 373–376. https://doi.org/10.1126/science.277.5324.373.
45. Oddo, S. (2008). The ubiquitin-proteasome system in Alzheimer's disease. J. Cell Mol. Med. *12*, 363–373. https://doi.org/10.1111/j.1582-4934.2008.00276.x.
46. Vagnucci, A.H., Jr., and Li, W.W. (2003). Alzheimer's disease and angiogenesis. Lancet (London, England) *361*, 605–608. https://doi.org/10.1016/S0140-6736(03)12521-4.
47. Inestrosa, N.C., and Varela-Nallar, L. (2014). Wnt signaling in the nervous system and in Alzheimer's disease. J. Mol. Cell Biol. *6*, 64–74. https://doi.org/10.1093/jmcb/mjt051.
48. Tesseur, I., Zou, K., Esposito, L., Bard, F., Berber, E., Can, J.V., Lin, A.H., Crews, L., Tremblay, P., Mathews, P., et al. (2006). Deficiency in neuronal TGF-beta signaling promotes neurodegeneration and Alzheimer's pathology. J. Clin. Invest. *116*, 3060–3069. https://doi.org/10.1172/JCI27341.
49. O' Neill, C. (2013). PI3-kinase/Akt/mTOR signaling: impaired on/off switches in aging, cognitive decline and Alzheimer's disease. Exp. Gerontol. *48*, 647–653. https://doi.org/10.1016/j.exger.2013.02.025.
50. Masliah, E., Mallory, M., Alford, M., Deteresa, R., and Saitoh, T. (1995). PDGF is associated with neuronal and glial alterations of Alzheimer's disease. Neurobiol. Aging *16*, 549–556. https://doi.org/10.1016/0197-4580(95)00050-o.
51. Baki, L., Marambaud, P., Efthimiopoulos, S., Georgakopoulos, A., Wen, P., Cui, W., Shioi, J., Koo, E., Ozawa, M., Friedrich, V.L., Jr., and Robakis, N.K. (2001). Presenilin-1 binds cytoplasmic epithelial cadherin, inhibits cadherin/p120 association, and regulates stability and function of the cadherin/catenin adhesion complex. Proc. Natl. Acad. Sci. USA *98*, 2381–2386. https://doi.org/10.1073/pnas.041603398.
52. Heinz, S., Benner, C., Spann, N., Bertolino, E., Lin, Y.C., Laslo, P., Cheng, J.X., Murre, C., Singh, H., and Glass, C.K. (2010). Simple

combinations of lineage-determining transcription factors prime cis-regulatory elements required for macrophage and B cell identities. Mol. Cell *38*, 576–589. https://doi.org/10.1016/j.molcel.2010.05.004.

53. Penicud, K., and Behrens, A. (2014). DMAP1 is an essential regulator of ATM activity and function. Oncogene *33*, 525–531. https://doi.org/10.1038/onc.2012.597.
54. Tian, B., Yang, Q., and Mao, Z. (2009). Phosphorylation of ATM by Cdk5 mediates DNA damage signalling and regulates neuronal death. Nat. Cell Biol. *11*, 211–218. https://doi.org/10.1038/ncb1829.
55. Pandita, T.K., Lieberman, H.B., Lim, D.S., Dhar, S., Zheng, W., Taya, Y., and Kastan, M.B. (2000). Ionizing radiation activates the ATM kinase throughout the cell cycle. Oncogene *19*, 1386–1391. https://doi.org/10.1038/sj.onc.1203444.
56. Dumont, M., and Beal, M.F. (2011). Neuroprotective strategies involving ROS in Alzheimer disease. Free Radic. Biol. Med. *51*, 1014–1026. https://doi.org/10.1016/j.freeradbiomed.2010.11.026.
57. Tsai, L.H., Lee, M.S., and Cruz, J. (2004). Cdk5, a therapeutic target for Alzheimer's disease? Biochim. Biophys. Acta *1697*, 137–142. https://doi.org/10.1016/j.bbapap.2003.11.019.
58. Rodríguez-Paredes, M., and Esteller, M. (2011). Cancer epigenetics reaches mainstream oncology. Nat. Med. *17*, 330–339. https://doi.org/10.1038/nm.2305.
59. Arrowsmith, C.H., Bountra, C., Fish, P.V., Lee, K., and Schapira, M. (2012). Epigenetic protein families: a new frontier for drug discovery. Nat. Rev. Drug Discov. *11*, 384–400. https://doi.org/10.1038/nrd3674.
60. Su, J., Wang, F., Cai, Y., and Jin, J. (2016). The Functional Analysis of Histone Acetyltransferase MOF in Tumorigenesis. Int. J. Mol. Sci. *17*, 99. https://doi.org/10.3390/ijms17010099.
61. Han, Z., Wu, H., Kim, S., Yang, X., Li, Q., Huang, H., Cai, H., Bartlett, M.G., Dong, A., Zeng, H., et al. (2018). Revealing the protein propionylation activity of the histone acetyltransferase MOF (males absent on the first). J. Biol. Chem. *293*, 3410–3420. https://doi.org/10.1074/jbc.RA117.000529.
62. Sayre, L.M., Perry, G., and Smith, M.A. (2008). Oxidative stress and neurotoxicity. Chem. Res. Toxicol. *21*, 172–188. https://doi.org/10.1021/tx700210j.
63. Li, Y., Huang, H., Zhu, M., Bai, H., and Huang, X. (2021). Roles of the MYST Family in the Pathogenesis of Alzheimer's Disease via Histone or Non-histone Acetylation. Aging Dis. *12*, 132–142. https://doi.org/10.14336/AD.2020.0329.
64. Li, Y., Huang, H., Zhu, M., Bai, H., and Huang, X. (2021). Roles of the MYST Family in the Pathogenesis of Alzheimer's Disease via Histone or Non-histone Acetylation. Aging Dis. *12*, 132–142. https://doi.org/10.14336/AD.2020.0329.
65. Ma, L.Y., Lv, Y.L., Huo, K., Liu, J., Shang, S.H., Fei, Y.L., Li, Y.B., Zhao, B.Y., Wei, M., Deng, Y.N., and Qu, Q.M. (2017). Autophagy-lysosome dysfunction is involved in Aβ deposition in STZ-induced diabetic rats. Behav. Brain Res. *320*, 484–493. https://doi.org/10.1016/j.bbr.2016.10.031.
66. Sakamaki, J.I., Wilkinson, S., Hahn, M., Tasdemir, N., O'Prey, J., Clark, W., Hedley, A., Nixon, C., Long, J.S., New, M., et al. (2017). Bromodomain Protein BRD4 Is a Transcriptional Repressor of Autophagy and Lysosomal Function. Mol. Cell *66*, 517–532.e9. https://doi.org/10.1016/j.molcel.2017.04.027.
67. Cavalli, G., and Paro, R. (1998). The Drosophila Fab-7 chromosomal element conveys epigenetic inheritance during mitosis and meiosis. Cell *93*, 505–518. https://doi.org/10.1016/s0092-8674(00)81181-2.
68. Cavalli, G., and Paro, R. (1999). Epigenetic inheritance of active chromatin after removal of the main transactivator. Science (New York, N.Y.) *286*, 955–958. https://doi.org/10.1126/science.286.5441.955.
69. Katz, D.J., Edwards, T.M., Reinke, V., and Kelly, W.G. (2009). A C. elegans LSD1 demethylase contributes to germline immortality by reprogramming epigenetic memory. Cell *137*, 308–320. https://doi.org/10.1016/j.cell.2009.02.015.
70. Ng, S.F., Lin, R.C.Y., Laybutt, D.R., Barres, R., Owens, J.A., and Morris, M.J. (2010). Chronic high-fat diet in fathers programs β-cell dysfunction in female rat offspring. Nature *467*, 963–966. https://doi.org/10.1038/nature09491.
71. Robison, A.J., and Nestler, E.J. (2011). Transcriptional and epigenetic mechanisms of addiction. Nat. Rev. Neurosci. *12*, 623–637. https://doi.org/10.1038/nrn3111.
72. Chan, T.L., Yuen, S.T., Kong, C.K., Chan, Y.W., Chan, A.S.Y., Ng, W.F., Tsui, W.Y., Lo, M.W.S., Tam, W.Y., Li, V.S.W., and Leung, S.Y. (2006). Heritable germline epimutation of MSH2 in a family with hereditary nonpolyposis colorectal cancer. Nat. Genet. *38*, 1178–1183. https://doi.org/10.1038/ng1866.
73. Hitchins, M.P., Wong, J.J.L., Suthers, G., Suter, C.M., Martin, D.I.K., Hawkins, N.J., and Ward, R.L. (2007). Inheritance of a cancer-associated MLH1 germ-line epimutation. N. Engl. J. Med. *356*, 697–705. https://doi.org/10.1056/NEJMoa064522.
74. Bohacek, J., and Mansuy, I.M. (2013). Epigenetic inheritance of disease and disease risk. Neuropsychopharmacology *38*, 220–236. https://doi.org/10.1038/npp.2012.110.
75. Bohacek, J., Gapp, K., Saab, B.J., and Mansuy, I.M. (2013). Transgenerational epigenetic effects on brain functions. Biol. Psychiatry *73*, 313–320. https://doi.org/10.1016/j.biopsych.2012.08.019.
76. Li, J., and Le, W. (2013). Modeling neurodegenerative diseases in Caenorhabditis elegans. Exp. Neurol. *250*, 94–103. https://doi.org/10.1016/j.expneurol.2013.09.024.
77. Fraser, A.G., Kamath, R.S., Zipperlen, P., Martinez-Campos, M., Sohrmann, M., and Ahringer, J. (2000). Functional genomic analysis of C. elegans chromosome I by systematic RNA interference. Nature *408*, 325–330. https://doi.org/10.1038/35042517.
78. Renaud, E., Barascu, A., and Rosselli, F. (2016). Impaired TIP60-mediated H4K16 acetylation accounts for the aberrant chromatin accumulation of 53BP1 and RAP80 in Fanconi anemia pathway-deficient cells. Nucleic Acids Res. *44*, 648–656. https://doi.org/10.1093/nar/gkv1019.

STAR★METHODS

KEY RESOURCES TABLE

REAGENT or RESOURCE	SOURCE	IDENTIFIER
Antibodies		
MOF	Bethyl Laboratories	CAT# A300-992A; RRID:AB_3170185
H4K16 (H4K16ac)	PTM Biolabs	CAT# PTM-122; RRID:AB_3170228
histone H3	Cell Signaling Technology	CAT# 9715; RRID:AB_331563.
β actin	Abcam	CAT# mAbcam 8224; RRID:AB_449644
Bacterial and virus strains		
E. coli OP50	Caenorhabditis Genetics Center	N/A
C.elegans RNAi Library	Source BioScience	N/A
Chemicals, peptides, and recombinant proteins		
Thioflavin T	Sigma-Aldrich	CAT# 596200; CAS:2390-54-7
LysoTracker red	Med Chem Express	CAT# HY-D1300; CAS: 231946-72-8
MG149	Sigma-Aldrich	CAT# SML3011; CAS: 1243583-85-8
AZD0156	Med Chem Express	CAT# HY-100016; CAS: 1821428-35-6
Uric acid	Sigma-Aldrich	CAT# U0881; CAS: 69-93-2
chloroquine diphosphate(CHQ)	Sigma-Aldrich	CAT# 1118000; CAS: 50-63-5
Roscovitine	Sigma-Aldrich	CAT# 557360; CAS:186692-46-6
Deposited data		
Chip-seq and RNA-seq data	Mendeley Data, V1	https://data.mendeley.com/datasets/pwkdk92sb4/1 https://doi.org/10.17632/pwkdk92sb4.1
Experimental models: cell lines		
SH-SY5Y	ATCC	CAT#CRL-2266; RRID:CVCL_0019
Experimental models: organisms/strains		
Strain CL802	Caenorhabditis Genetics Center	*smg-1(cc546);rol-6(su1006)*
Strain CL4176	Caenorhabditis Genetics Center	*smg-1(cc546ts)*;dvIs27(*myo-3*p::A-Beta (1–42):*let-851* 3′UTR) + *rol-6(su1006)*
Strain CL2331	Caenorhabditis Genetics Center	*myo-3*p::GFP::A-Beta (3–42) + *rol-6(su1006)*
Strain VC1931	Caenorhabditis Genetics Center	*mys-2(ok2429)*
CL4176;*mys-2(ok2429)*	This paper	N/A
Oligonucleotides		
mys-2 RNAi verification primer: (forward)TTTCAGAAGAAGGGATACGG (reverse)GTCGCCACCACCAATAGC	This paper	N/A
actin primer: (forward)CCCAGAGG AACACCCAGTTC (reverse)CACCATCTCCGGTGTCCAAA	This paper	N/A
mys-2 promoter primer: (forward) CTAGAGGATCCCCGGCAAAATT TTCAGGTTCTAATGTCTG (reverse) TTTGGCCAATCCCGGCA TTTTGTCTGGAAATTTTTGCTG.	This paper	N/A

(*Continued on next page*)

Continued

REAGENT or RESOURCE	SOURCE	IDENTIFIER
Aβ1-42 (*APP*) primer: (forward)CCGACATGACTCAGGATATGAAGT (reverse)CACCATGAGTCCAATGATTGCA	This paper	N/A
CL4176;*mys-2(ok2429)* verification primer: (forward)TCCATGTCTATCTTGGCCGC (reverse)AATCTCGTGAGCGCCTATCG	This paper	N/A
ilys-2 primer: (forward)TCCGCCGATTGTCTCCATT (reverse)AGCACATCTCTTCCAGGCA	This paper	N/A
ttr-41 primer: (forward)GAAGCACCCACGAGCTTACT (reverse)TGCTCATCAGTTGGGGTTCC	This paper	N/A
Chip qPCR primer	This paper	Table S3
Software and algorithms		
KEGG Analysis	DAVID database	https://david.ncifcrf.gov/
RNA-seq Illumina HiSeq 2000 system	Vazyme Biotech platform	https://www.vazymeglobal.com/
Chip-seq Analysis	Wuhan Seq Health Technology Co. Ltd.	https://seqhealth.cn/
Analysis of MOF expression in AD patient	Alzdata	http://www.alzdata.org/index.html
Other		
EpiQuik Total Histone Extraction Kit	EpiGentek, New York, NY	CAT #OP-0006-100
siRNA Transfection Reagent	Santa Cruz	CAT #sc-29528
SimpleChIP® Plus Enzymatic Chromatin IP Kit (Magnetic Beads)	Cell Signaling Technology	CAT #9005

RESOURCE AVAILABILITY

Lead contact

Further information and requests for resources and reagents should be directed to and will be fulfilled by lead contact, Xiaowei Huang (xwhuang@ynu.edu.cn).

Materials availability

This study did not generate new unique reagents.

Data and code availability

- The Chip-seq and RNA-seq data in this study are openly available in Mendeley Data. The DOI is listed in the key resources table. This paper analyzes the publicly available data. These websites for the datasets are listed in the key resources table. The other data reported in paper and supplementary will be shared by the lead contact upon reasonable request.
- This paper does not report original code.
- Any additional information required to reanalyze the data reported in this paper is available from the lead contact upon request.

EXPERIMENTAL MODEL AND STUDY PARTICIPANT DETAILS

C. elegans strain and culture

Aβ-transgenic *C. elegans* CL4176 [genotype *smg-1(cc546ts)*; dvIs27(*myo-3*p::A-Beta (1–42):*let-851* 3′UTR) + *rol-6(su1006)*] and CL2331 [*myo-3*p::GFP::A-Beta (3–42) + *rol-6(su1006)*], and their negative control CL802 [*smg-1(cc546); rol-6(su1006)*] which did not express Aβ, were obtained from the Caenorhabditis Genetics Center (CGC) and maintained on nematode growth media (NGM) plates seeded with the food bacteria, *Escherichia coli* OP50, at 16°C. The drug treatments were performed in L3 stage of worm until laying eggs.

To explore the potential epigenetic effects, we propagated synchronized transgenic nematode CL4176 L1 larvae on plates. The plates were then incubated with HT115 carrying the blank vector L4440, or *mys-2* RNAi at 16°C until the nematodes had laid a sufficient quantity of eggs. Twenty to thirty gravid adults were selected using a platinum worm picker, then transferred to NGM plates with fresh *E. coli* OP50. Therefore, we allowed these nematodes to lay eggs for 2 h at 16°C. The gravid adults were then removed, and the progeny (F1)

were allowed to grow for another 72 h. We then raised the temperature to 25°C to induce Aβ1–42 overexpression and counted the rates of paralysis every 2 h. We assayed the F2 progeny in the same way.

Cell line

The cell lines SH-SY5Y were purchased from ATCC (RRID: CVCL_0019) and cultured in DMEM medium with 10% serum in a cell incubator containing 5% CO_2 at 37°C.

METHOD DETAILS

Paralysis assay

Paralysis assays were performed as described previously (Dostal et al., 2010). Gravid adult worms were placed on NGM plates spread with food bacteria and allowed to lay eggs for 2 h at 16°C. Then, the adults were removed and the eggs were allowed to hatch and grow at 16°C. Approximately 50 progenies were maintained on each plate and incubated at 16°C for 36 h until the third larval stage (L3). The nematodes were then transferred to NGM plates at 25°C, and those that remained immobile after prodding were counted as paralyzed. In addition, CL802 as the negative controls were cultured via the same methods as those described for CL4176 nematodes.

RNAi protocol

RNAi in *C. elegans* was administered using a feeding method described in a previous report[77] with RNAi clone in the *C.elegans* RNAi Library (Source BioScience, UK). Target genes were knocked down by feeding the nematodes *E. coli* HT115 (DE3) bacteria carrying target-gene dsRNAs. The specified RNAi clone *E. coli* was seeded onto NGM agar plates supplemented with 50 μg/mL ampicillin and 1 mM β-D-1-thiogalactopyranoside (IPTG). Then, dsRNA expression was induced by IPTG overnight at room temperature. Synchronized populations of L1 larvae were fed by bacteria expressing dsRNA until they reached the L4 stage. HT115 bacteria carrying an empty L4440 vector were used as a negative control.

Cell transfection was performed using the siRNA reagent and siRNA (Santa Cruz, Texas, USA), using the traditional antibiotic screening method follow the reagent protocol.

Staining of Aβ and lysosome

Thioflavin T (Sigma, MA, USA) were used for Aβ staining. After increasing the temperature from 16°C to 25°C, the CL4176 were allowed to grow for 28 h. The nematodes were then washed once with phosphate-buffered saline (PBS) and collected into microfuge tubes. Following removal of the supernatant by centrifugation at 3,000 rpm for 3 min, we transferred the centrifuged nematodes to 1 mL of 4% formaldehyde. The nematodes were kept at 4°C for 24 h. The nematodes were then stained in 20 mM Thioflavin T in 50% alcohol at 4°C for 24 h. Then, the stained nematodes were decolorized using an ethanol gradient (50, 75, and 90%). Fluorescence from Aβ stained with Thioflavin T was monitored using excitation at 440 nm and emission at 482 nm.

The lysosome of *C. elegans* and cells were staining with LysoTracker red (MCE, Shanghai, China). 50 nM staining solution were incubated with the worms or cells at room temperature for 60 min. Wash to remove the redundant staining solution, and the fluorescence indicated lysosomes can be monitored using excitation at 540 nm and emission at 605 nm.

ELISA analysis of Aβ

In each group, about 100 worms were collected and washed by M9 buffer to remove bacteria away. They were lysed in lysis buffer containing protease inhibitors with ultrasonic crushing. After centrifugation at 12,000 g for 5 min, the supernatant and Aβ1-42 standard were dispensed into the wells of the ELISA plate (Elabscience, Wuhan, China). According to assay procedure, the optical density (O.D.) of each well at 450 nm were read after incubation. The content of Aβ1-42 was calculated according to the standard curve of the synchronous test.

Western blotting

Total histones were extracted using an EpiQuik Total Histone Extraction Kit (EpiGentek, New York, NY). After separation for 90 min on a 12% SDS-PAGE gel at 150 V, the proteins were electrophoretically transferred to a polyvinylidene-difluoride (PVDF) membrane for 60 min using a Mini Bio-Rad Trans-Blot system at 200 mA. After blocking overnight at 4°C with 5% bovine serum albumin (BSA) in PBS, we incubated the PVDF membranes with primary antibodies against MOF (Bethyl, Texas, USA) or acetylated histone H4K16 (H4K16ac) (PTM Biolabs Inc., Chicago, IL, USA) at 1:1,000 dilutions for 2 h at room temperature. The membranes were then incubated with horseradish-peroxidase-conjugated anti-rabbit secondary antibody (1:5,000 dilution) for 1 h at room temperature. We then used ECL reagent to produce chemiluminescent signals that were detected using an Amersham Imager 600 system (GE, MA, USA). Antibodies against actin (Abcam, Cambridge, UK) or histone H3 (CST, MA, USA) were used as the controls of Western blotting.[78]

RNA-seq

For sample preparation of RNA-seq, P0 generation group [CL4176 and CL4176;*mys-2(ok2429)*] worms were synchronized and maintained on each plate and incubated at 16°C for 36 h until the third larval stage (L3). Then transfer to 25°C 24 h to induce Aβ1-42. For F1 generation group,

the offsprings of CL4176;*mys-2* RNAi and its control worms were collected without RNAi in F1 progeny but Aβ induce treatment. At least 1,000 worms were collected for each sample. All worms were washed several times with M9 buffer to remove bacteria, then frozen in Qiazol (QIAGEN, Germany)) for RNA isolation. RNA was extracted with Trizol reagent according to the manufacturer's instructions. RNA concentrations and quality were determined using a Nanodrop system. Only RNA samples with RIN >8.0 and 18S/28S > 1.0 were used for library preparation. Sequencing was performed using an Illumina HiSeq 2000 system (Vazyme Biotech). To analyze RNA-seq data, the reads were first trimmed and mapped to the WS256 genome (from Worm Base) using STAR (version 2.5) and Rsubread. Then, we performed sequence alignment analysis using Hisat2 with reference sequences. Based on the comparison results of Hisat2, cufflinks analysis was used to quantitate gene expression. We used the cuffdiff analysis module of cufflinks to determine differential gene expression among the samples. The criteria for differentially expressed gene screening were $|\log2Ratio| \geq 1$ and q value ≤ 0.05. Finally, based on the results of differential expression analysis, GO term and KEGG pathway enrichment analyses were performed using the DAVID platform.

Chromatin-immunoprecipitation sequencing (ChIP-seq) and ChIP–quantitative polymerase chain reaction (ChIP-qPCR)

ChIP-seq and ChIP-qPCR were performed using a Simple ChIP Plus Enzymatic Chromatin IP Kit (Cell Signaling Technology, MA, USA) according to the manufacturer's instructions. ChIP-seq was designed to identify MOF interactions with DNA. The reaction was performed in AD model SHSY-5T adding with Aβ for 24 h. ChIP-qPCR was performed on candidate genes from CL4176, CL4176;*mys-2* RNAi in P0 and its F1 progeny. The primers were listed in Table S3. For each ChIP reaction, the lysate was incubated with anti-MOF (Bethyl, Texas, USA) and anti-H4K16ac (PTM Biolabs Inc., Chicago, IL, USA) and shaken at 4°C overnight. We incubated beads with rabbit IgG as a negative control for nonspecific genomic DNA binding. Immune complexes were precipitated with protein G, then washed with low-salt immune-complex wash buffer, high-salt immune-complex wash buffer, LiCl immune-complex wash buffer, and two washes in TE buffer. The bound protein was eluted in 1% SDS and 0.1 M $NaHCO_3$. After reversing crosslinking by heating at 65°C for 2 h, we purified DNA using spin columns to produce samples for either sequencing or qPCR. ChIP-seq was performed by Wuhan Seq Health Technology Co. Ltd.

To quantify the amount of immunoprecipitated DNA by qPCR, we expressed the signals obtained from each immunoprecipitation as a percent of the total input chromatin, as follows:

$$Percent\ Input\ =\ 2\%\ x2^{\left(C[T]\ 2\%Input\ Sample\ -\ C[T]\ IP\ Sample\right)};\ \text{and}$$

$$C\ [T]\ =\ CT\ =\ \text{Threshold cycle of PCR reaction.}$$

Localization of *mys-2* expression

Infusion primers for cloning the *mys-2* promoter were list in key resources table. The amplified *mys-2* promoter was linked to the plasmid pPD95_79 that contained GFP in frame. The recombinant plasmid was microinjected into the CL4176 germline and the nematodes were then cultivated on NGM medium until the L4 larval stage. The F1 generation that had GFP fluorescence was chosen to localize the expression pattern of *mys-2*.

QUANTIFICATION AND STATISTICAL ANALYSIS

Each dataset was collected from at least three biological replicates. The percent of mobile (non-paralyzed) nematodes are presented as the mean ± SE. All other results are expressed as the mean ± standard deviation (SD). Fluorescence quantified from 10 to 20 nematodes. Statistical comparisons were performed using one-way or two-way analysis of variance (ANOVA) and Student's t-test or multiple unpaired t tests. The log rank test was applied in the non-paralyzed rates comparation. *$p < 0.05$; **$p < 0.01$; ***$p < 0.001$; ***$p < 0.0001$.